NBSIR 84-3010

COMPARISON OF MEASURED AND CALCULATED MUTUAL COUPLING IN THE NEAR FIELD BETWEEN MICROWAVE ANTENNAS

National Bureau of Standards
U.S. Department of Commerce
Boulder, Colorado 80303

June 1984

NBSIR 84-3010

COMPARISON OF MEASURED AND CALCULATED MUTUAL COUPLING IN THE NEAR FIELD BETWEEN MICROWAVE ANTENNAS

Carl F. Stubenrauch
Michael H. Francis

Electromagnetic Fields Division
National Engineering Laboratory
National Bureau of Standards
U.S. Department of Commerce
Boulder, Colorado 80303

June 1984

Prepared for:
Department of Defense
Electromagnetic Compatibility Analysis Center
Annapolis, Maryland 21402

U.S. DEPARTMENT OF COMMERCE, Malcolm Baldrige, Secretary

NATIONAL BUREAU OF STANDARDS, Ernest Ambler, Director

CONTENTS

Comparison of Measured and Calculated Mutual Coupling in the Near Field Between Microwave Antennas

Carl F. Stubenrauch and Michael H. Francis

National Bureau of Standards
Boulder, Colorado 80303

Measurements of near-field mutual coupling were performed between two moderate sized microwave antennas and compared to coupling calculated using recently developed computer programs. Input data for the programs are the complex far-field radiation patterns of the antennas. Experimentally determined and calculated coupling as a function of both transverse displacement and separation agree closely except for a constant offset observed in some cases. In addition, coupling values computed using a program which approximates the far-field radiation patterns were compared to experiment and found to be satisfactory.

Key words: co-sited antennas, coupling loss, far fields, mutual coupling, near fields.

1. Introduction

Recent theoretical work at the National Bureau of Standards has led to the development of computer programs which can efficiently calculate the coupling loss between two antennas regardless of their separation. Thus near-field as well as far-field coupling may be calculated [1].

The required data for the calculation are the far-field patterns (amplitude and phase) for the two antennas, and the geometrical factors which define the relative orientations and separation of the two antennas.

Two computer programs have been developed which calculate the coupling loss, b'_0/a_0, between two antennas as a function of transverse displacement and as a function of radial displacement. b'_0 is the amplitude of the wave emerging from the waveguide feed of the receiving antenna and a_0 is the amplitude of the wave incident in the waveguide feed of the transmitting antenna, as illustrated in figure 1. The program CUPLNF, which calculates coupling versus transverse displacement, was documented previously [2]. Program CUPLZ, for coupling versus longitudinal displacement, is discussed in [1].

It is the purpose of this study to compare coupling losses measured for a variety of geometrical situations to the corresponding losses calculated using the computer programs. Measurements were performed using the NBS near-field scanner and data were obtained for both transverse and radial displacements. Far-field patterns used in the calculation of coupling loss were obtained from transformed planar near-field measurements [5].

In addition, results are presented comparing measured coupling and coupling calculated from program ENVLP [3] which uses estimated far-field patterns rather than exact far-field patterns for the calculations.

2. Description of Measurement Procedure

In order to experimentally verify the coupling formulation, coupling between two pairs of antennas was measured. The first antenna was a 1.2 meter paraboloidal reflector antenna having a power gain of approximately 30 dB and a half-power beamwidth of 4.5° (fig. 2a). The second antenna was a 25-element microstrip array having a power gain of approximately 22 dB and a half-power beamwidth of 15° (fig. 2b). Most of the coupling measurements were performed on this antenna pair. Some preliminary tests were also performed to measure the coupling between the reflector antenna and an open-ended section of WR187 waveguide of the type which is often used as the probe antenna in near-field measurements.

Far-field radiation patterns necessary for the calculation of near-field coupling were obtained from probe-corrected near-field measurements on the reflector and array antennas. The far-field pattern of the open-ended waveguide was measured directly.

The region over which a valid far-field pattern is obtained using near-field techniques is determined by the aperture size and scan areas as was shown by the error analysis of Yaghjian [4] and the experimental work of Newell and Crawford [5]. From this work it can be demonstrated that the patterns for the antennas used are valid to an angle of approximately 60° off boresight for the reflector antenna and 77° off boresight for the array antenna. The waveguide probe pattern is valid over the entire forward hemisphere. The patterns for the three antennas are shown in figures 3 through 5.

Measurements were performed at the NBS near-field measurement facility which allows precise adjustment and determination of the relative orientation of the two antennas. The reflector antenna was mounted on a rotator which allowed rotation of the antenna about a vertical axis. This rotator was mounted on a movable cart which travels on a pair of precision rails which are aligned to be perpendicular to the plane of the near-field scanner thus allowing variation of the separation distance between the two antennas.

The second antenna, either the microstrip array or the waveguide probe, was mounted on the x-y positioner of the NBS near-field scanner. The antennas were carefully aligned so that the relationship between the coordinate systems in which the far-field patterns of the antennas were obtained and the common coordinate system could be accurately determined. Two wedges were also employed in mounting the array antenna which allowed it to be rotated by angles of 21.6° and 30.3° about a vertical axis.

In all cases, the polarization vectors for the antennas were parallel and oriented in the y-direction. The current versions of the coupling programs only calculate coupling due to a single component of the far field of each antenna. Hence, one can only calculate meaningful coupling values for coupling where the polarization vectors are parallel. Because of this limitation, no coupling measurements were made for cases where the antennas were oriented with their polarization vectors orthogonal.

The measurements were performed for coupling loss as a function of x and y position for various values of θ_T and θ_R, where θ_T and θ_R are the angles by which the transmitting or receiving antenna boresight direction is rotated with respect to the common coordinate system as illustrated in figure 6. Measurements were also performed for coupling as a function of separation for various values of θ_T and θ_R. The comparison between measured and calculated coupling will be discussed in section 3 for transverse displacement and in section 4 for longitudinal displacement.

In section 5, we discuss comparisons made between measurements and calculations using approximate far field radiation patterns and program ENVLP.

3. Coupling Loss Versus Transverse Displacement

We briefly state here the major result of the mathematical development in order to be able to discuss the results. It has been shown by Yaghjian [1] and [2] that the coupling between two antennas, neglecting multiple reflections, is given by,

$$\frac{b_o'(\underline{R})}{a_o} = -C' \iint_{K<k} \frac{\underline{f}(\underline{k}) \cdot \underline{f}'(-\underline{k}) e^{i\gamma d} e^{i\underline{K}\cdot\underline{R}}}{\gamma} d\underline{K} \qquad (1)$$

where C' is a constant which includes the mismatch correction and $\underline{f}$ and $\underline{f}'$ are the free space, far electric field radiation pattern of the transmitting and receiving antennas respectively. The propagation vector is $\underline{k} = k_x \hat{e}_x + k_y \hat{e}_y \pm \gamma \hat{e}_z = \underline{K} \pm \gamma \hat{e}_z$. $|k| = 2\pi/\lambda$ with λ the wavelength. The location of the receiving antenna in the common coordinate system is $\underline{r} = \underline{R} + d\,\hat{e}_z$. The $e^{-i\omega t}$ time convention is employed throughout.

Yaghjian has also shown that, for most cases, the integration range may be limited to $K/k < (D_T + D_R)/d$ where D_T and D_R are the diameters of the smallest spheres circumscribing the radiating part of each antenna (including feeds, struts, edges and all other parts of the antennas which radiate or affect the reception significantly). This range should give good results for $|R| < (D_T + D_R)$. This restriction of the integration range also has the effect of artificially bandlimiting the integrand so that the sampling theorem may be applied. Two parameters, XLIM and BFAC, control the actual integration range and increment employed in the program. The actual integration range is

$$\frac{K_{max}}{k} = \left(\frac{D_T + D_R}{d}\right) \cdot \text{XLIM} \; . \qquad (2)$$

The actual increment value is

$$\frac{\Delta k_x}{k} = \frac{\Delta k_y}{k} = \frac{d}{(D_T + D_R) \cdot \text{XLIM}} \cdot \frac{1}{\text{BFAC}} \; . \qquad (3)$$

We also note that K_{max}/k is never allowed to exceed 0.9 in the program. This restriction of the integration limits amounts to making use of the fact that only those rays which originate from a point on one antenna and actually intersect a part of the other antenna take part in the interaction.

The measurements performed of coupling versus transverse displacement are summarized in table 1. The definition of the coordinate systems are illustrated in figure 6. In addition, for case 8, we illustrate the effect of the integration limit and increment on the results of the calculation.

For each set of relative cases, we present a plot of measured and calculated coupling loss for a transverse displacement in the two orthogonal directions, x and y. In all cases, rotations are about the y (vertical) axis. Polarization of each antenna is nominally vertical.

Rotations were limited to ± 30° for both the array and reflector antennas because rotation to angles greater than this would require a large angular segment of radiation pattern which could not be determined from the near-field measurements.

Agreement between measured and calculated coupling loss is very good for almost every case. It is noted that the magnitude of the measured, compared to the calculated curves, seems to diverge slowly as the antennas are turned so that their boresight direction deviates from the z-axis in the common coordinate system. In almost every case, the experimentally determined coupling is larger than the calculated coupling. The maximum discrepancy is approximately 3 dB. Considerable effort has been devoted to determine the cause of this systematic discrepancy, however, no cause has been determined.

We note that in cases 7 and 9, the calculated y-scan pattern does not match the measured data closely. In these cases the coupling loss is very large (> 45 dB). In the case of large coupling loss, one can no longer ignore the effect of coupling through the cross polarized components as is implicitly done by the computer program. Thus the discrepancy in these cases may be caused by cross polarization effects.

As is discussed in [1], the coupling calculation is valid for $|R| < (D_T + D_R)$ (= 1.4 meters for our case). The calculated coupling is generally good to this distance.

Finally, for case 8, we illustrate the effect of changing XLIM and BFAC. In all previously presented results, calculations were performed with XLIM = BFAC = 2. In figure 19 we see the same results as those illustrated in figure 14a only for various values of XLIM and BFAC. These results are typical of those obtained for the other cases. The agreement between the various curves is very good up to a transverse displacement of about 1 meter. Beyond 1 meter, the various examples diverge with the best result, as expected, being for XLIM and BFAC both set to 2. We see that the results for XLIM = 1, BFAC = 2, and XLIM = 2, BFAC = 1 are essentially identical. This indicates that the size of the increment is more important than the range of the integral since for these two cases the increment is the same, but the limit is larger for the second case as can be seen from equations 2 and 3.

4. Coupling Loss Versus Separation

As for the transverse case, we begin by briefly reviewing the mathematical results relating to the calculation of coupling versus longitudinal displacement. As has been discussed by Yaghjian [1], the calculation may not be completed by simply performing the γ transform of (1) because the necessary increment size requires impractical array sizes and computation time. However, the coupling loss satisfies the scalar wave equation, and, as a result, can be expressed in terms of spherical wave functions. Further, since the choice of the polar axis is arbitrary, the longitudinal axis may be chosen as the polar axis with the resulting simplified expression for the coupling:

$$\frac{b_o'(d)}{a_o} = \sum_{n=o}^{\infty} B_n \, h_n^{(1)}(kd), \quad d > (D_T + D_R)/2 \tag{4}$$

where we have

$$B_n = \frac{(2n+1)}{2} (i)^n \int_0^{\pi} \int_0^{2\pi} \underline{f}' \cdot \underline{f} \, P_n(\cos\theta_o) \sin\theta_o d\phi_o d\theta_o \, . \qquad (5)$$

$h_n^{(1)}$ is the spherical Hankel function of the first kind which represents outgoing waves with the chosen time convention and $P_n(\cos\theta)$ is the Legendre polynomial.

A program, CUPLZ, was written to calculate the coupling loss between two antennas as a function of longitudinal displacement employing the above theory. As originally written, the input data for the far field radiation patterns were obtained from a mathematical model for the antenna such as a uniformly distributed circular aperture. The program has been modified to obtain these patterns from an array of actual far-field patterns. The calculated coupling obtained from this modified program was compared to the experimentally obtained results.

These measurements are summarized in table 2. In all cases, the coupling loss was measured for a range of 1 meter to 4 meters. In general, all of the calculated curves match the measured curves except that an offset of 2 to 3 dB is again observed.

It is interesting to note the similarity between figures 22 and 25 and between figures 26 and 27. In these pairs of figures the angle θ_T, the angle by which the reflector antenna boresight is rotated from the common axis, is the same while θ_R, the corresponding angle for the array, is different. This occurs because the array aperture is considerably smaller than the reflector and most features of the coupling curve are due to the larger antenna with some slight modification by the smaller antenna.

5. Comparison of Program ENVLP to Experiment

Francis and Yaghjian [3] developed a computer program, ENVLP, to estimate the coupling between antennas when only the separation of the antennas, the electrical size of the antennas, and the side-lobe level of each antenna along the axis of separation are known and, in particular, detailed information on the far-field phase is unknown. Their results were compared to the exact coupling results obtained for two hypothetical antennas. In this section we compare the coupling results obtained from ENVLP to the experimental coupling results obtained using the microstrip array and the 1.2 m reflector antenna.

Five orientations of the two antennas were chosen so as to compare the results of ENVLP to the experimental results. These orientations are defined in table 3 below. For the first two orientations, all criteria as specified in [3] are met. For the third and fourth orientations of table 3, coupling involves parts of the main beams and for the last orientation, the two antennas are directly facing each other and, thus, the coupling involves mostly the main beams (Francis and Yaghjian gave as one of the conditions of using ENVLP that coupling not involve the main beam since ENVLP does not model the phase well in this region and, in addition, coupling involving large portions of the main beam will lead to variations in the amplitude of the envelope of the far field which is greater than 3 dB).

ENVLP computes the coupling along a line segment perpendicular to the separation axis (for details see Francis and Yaghjian [3]). From this, ENVLP finds the maximum coupling along the line

segment and the RMS Mean of the coupling along the line segment. In [3] it is concluded that the actual coupling of the antennas along the separation axis should be within about 10 dB of the computed maximum coupling and within ± 5 dB (plus the uncertainty in the side-lobe levels) of the computed RMS Mean coupling. The results for the five orientations of table 3 are found in table 4.

We see that the computed maximum coupling falls within the stated uncertainty for all the cases of table 3 and the computed RMS Mean falls within the stated uncertainty for all orientations except number 5. It is to be expected that the results of orientation 5 would not be within the stated uncertainty since it involves the main beams.

At first, it may appear surprising that results obtained for orientation 3 fall within the stated uncertainties of ENVLP since it involves coupling of the microstrip array main beam, although only part of the main beam. An examination of figure 28 shows that only a small part (about 11 percent) of the solid angle subtended by the dish is also subtended by the main beam. In addition, the maximum power level of that part of the main beam which sees the dish is only twice the maximum side-lobe power level. This explains why case 3 falls within the stated uncertainties of ENVLP.

It is surprising that case 4 meets the stated uncertainty since the dish sees the microstrip array only through its main beam. We conclude that it is only by chance that this occurs and such situations as case 4 should still be avoided in using ENVLP.

6. Conclusions and Suggestions for Further Work

It has been shown that the programs CUPLNF and CUPLZ give good results for predicting the coupling between two antennas in the near-field region. In particular, patterns for displacements in the transverse direction and the longitudinal direction show excellent agreement except when the coupling loss is high (> 45 dB). For some situations, a constant offset was observed, however, it is not great enough to affect the utility of the programs for electromagnetic compatibility purposes.

We find that for real antennas, the program ENVLP gives a computed maximum coupling which is within 10 dB (plus the uncertainty of the side-lobe levels) and a computed RMS Mean coupling which is within ± 5 dB (plus the uncertainty of the side-lobe levels) of the actual coupling along the separation axis provided that the conditions of Francis and Yaghjian [3] are met. In particular, ENVLP cannot be used to calculate the coupling between two antennas if more than about fifteen percent of the solid angle subtended by either antenna (as seen by the other) is also subtended by the main beam of the other antenna.

If it is desired to predict coupling to very low levels, or for the more general case where the antenna polarization vectors are not parallel, it will be necessary to include both polarization components of the far field.

Two areas mentioned above are worthy of further research or development. While results are good enough for compatibility applications, the cause of the discrepancy between the amplitude of the calculated and measured curves should be determined. Resolution of this difficulty may lead to increased understanding of the coupling problem.

We also recommend that the programs be modified to include coupling between non-parallel polarized antennas. While the task is not trivial because of the large amounts of data required

and the necessity of having both polarizations of both antennas to properly compute the dot product in (1) or (5), the increased usefulness and generality of the resultant programs would be of great use.

The authors wish to thank Dr. Arthur D. Yaghjian and Allen C. Newell of NBS for many helpful discussions, and Douglas P. Kremer and Douglas T. Tamura for performing the measurements. The support of Dr. Ramon C. Baird of NBS is also appreciated. The microstrip array antenna was provided by Ball Brothers Research Corporation. The work was sponsored by the Electromagnetic Compatibility Analysis Center of the Department of Defense.

7. References

[1] Yaghjian, A. D. Efficient computation of antenna coupling and fields within the near-field region. IEEE Trans. Antennas Propag., AP-30, pp. 113-128, 1982 January.

[2] Stubenrauch, C. F.; Yaghjian, A. D. Determination of mutual coupling between co-sited microwave antennas and calculation of near-zone electric field. Nat. Bur. Stand. (U.S.), NBSIR 80-1630, 1981 June.

[3] Francis, M. H.; Yaghjian, A. D. Computation of antenna sidelobe coupling in the near field using approximate far-field data. Nat. Bur. Stand. (U.S.), NBSIR 82-1674, 1982 August.

[4] Yaghjian, A. D. Upper-bound errors in far-field antenna parameters determined from planar near-field measurements, Part 1: Analysis. Nat. Bur. Stand. (U.S.), Tech. Note 667, 1975 October.

[5] Newell A. C.; Crawford, M. L. Planar near-field measurements on high performance array antennas. Nat. Bur. Stand. (U.S.), NBSIR 74-380, 1974 July.

Table 1. Cases studied for Coupling versus Transverse displacement

Case #	Antenna	θ_T (degrees)	θ_R (degrees)	d (meters)	Figure #
1	Probe	0	0	2	7a,b
2	Probe	20	0	2	8a,b
3	Probe	30	0	2	9a,b
4	Array	0	0	3	10a,b
5	Array	20	0	3	11a,b
6	Array	-30	-21.6	2	12a,b
7	Array	-20	-21.6	4	13a,b
8	Array	0	-21.6	3	14a,b
9	Array	20	-21.6	3	15a,b
10	Array	30	-21.6	2	16a,b
11	Array	0	-30.3	2	17a,b
12	Array	20	-30.3	4	18a,b

Note: Eulerian angles [1] for each case are not listed since the antennas have been rotated only about the y_A and y_P axes which remain parallel. Hence, for descriptive purposes, only the angles θ_T and θ_R need be specified. If θ_T is positive, then the Eulerian angles are $\phi_A = \psi_A = 0°$ and $\theta_A = \theta_T$. If θ_T is negative, the Eulerian angles become $\phi_A = \psi_A = 180°$, and $\theta_A = -\theta_T$. Similar relations hold between θ_R and the angles ϕ_P, θ_P, and ψ_P.

Table 2. Cases studied for Coupling versus Separation

Case #	Antenna	θ_T (degrees)	θ_R (degrees)	Figure #
1	Probe	10	0	20
2	Array	0	0	21
3	Array	20	0	22
4	Array	-20	-21.6	23
5	Array	10	-21.6	24
6	Array	20	-21.6	25
7	Array	30	-21.6	26
8	Array	30	-30.3	27

Table 3. Orientations studied for ENVLP

Orientation	θ_T (degrees)	θ_R (degrees)
1	30	-30.3
2	20	-30.3
3	20	-21.6
4	0	-21.6
5	0	0

Separation (all cases): 4.0 meters
Frequency (all cases): 4.0 GHz
Radius of microstrip array: 0.15 meters
Radius of reflector antenna: 0.61 meters

Table 4. Coupling results from ENVLP

Orientation	RMS Mean (dB)	Maximum (dB)	Experimental Result (dB)
1	-65.51	-59.14	-61.58
2	-53.51	-47.14	-57.91
3	-49.51	-43.14	-50.72
4	-31.48	-25.12	-28.50
5	-21.49	-15.12	-12.57

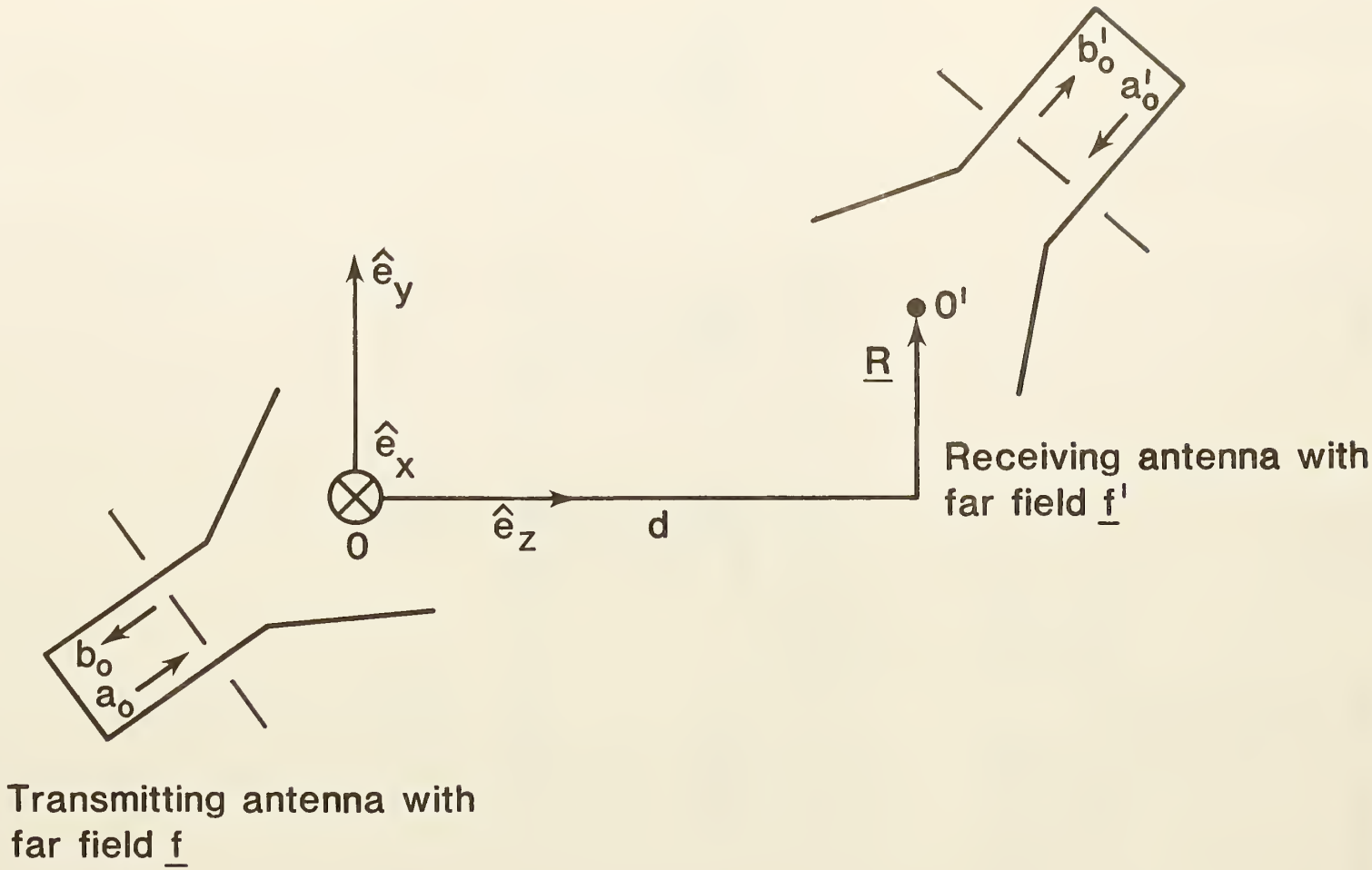

Figure 1. Schematic of two arbitrarily oriented and separated antennas. Coupling loss is $b_o'(\underline{R},d)/a_o$. For transverse displacement, d is held constant; for radial displacement, $\underline{R} = 0$.

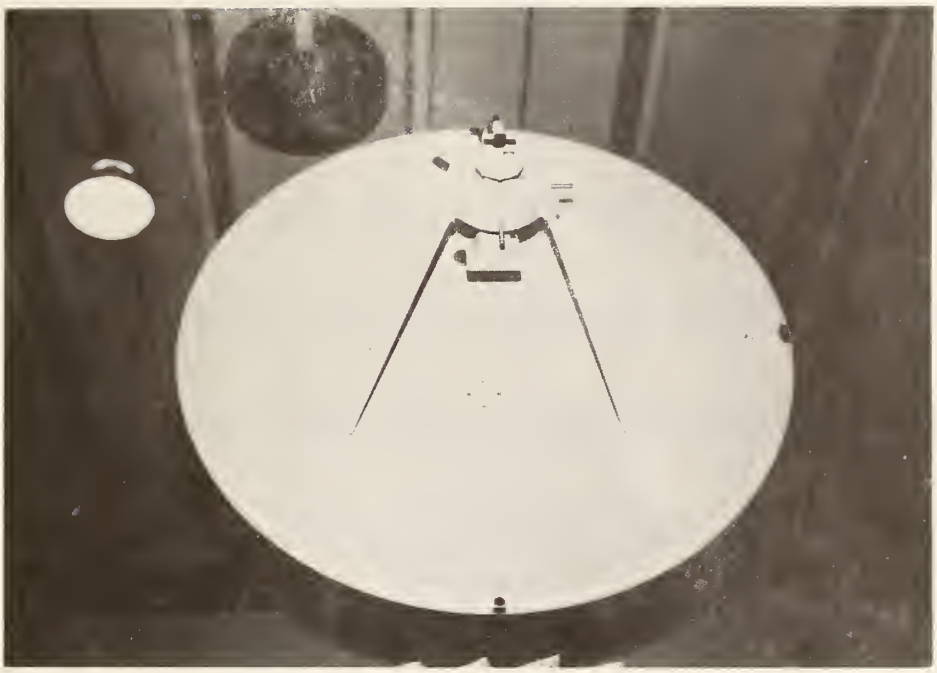

Figure 2a. Photograph of reflector antenna used in the coupling measurements.

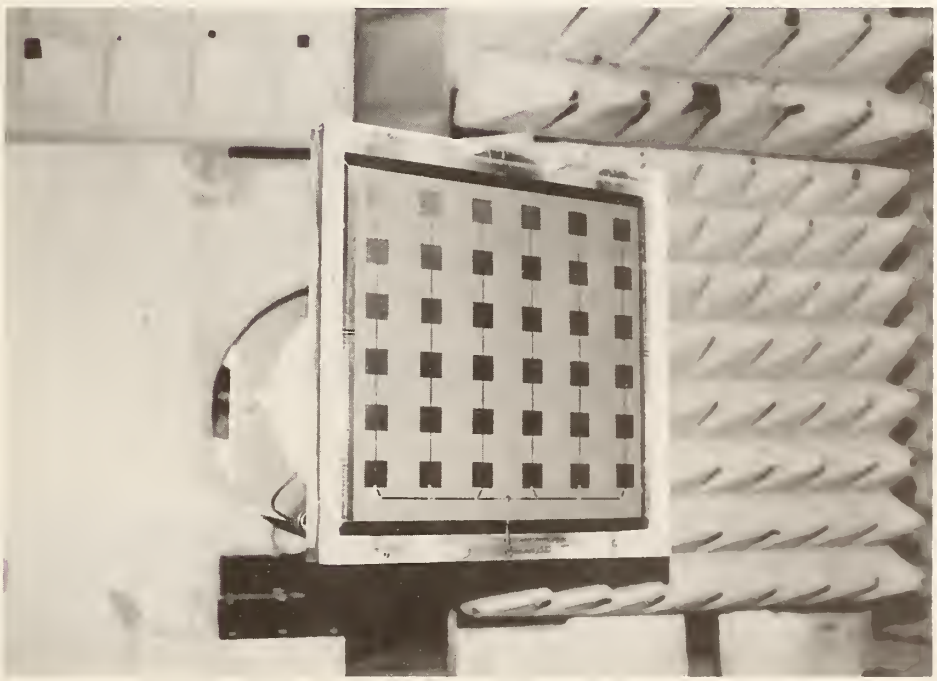

Figure 2b. Photograph of microstrip array antenna used in the coupling measurements.

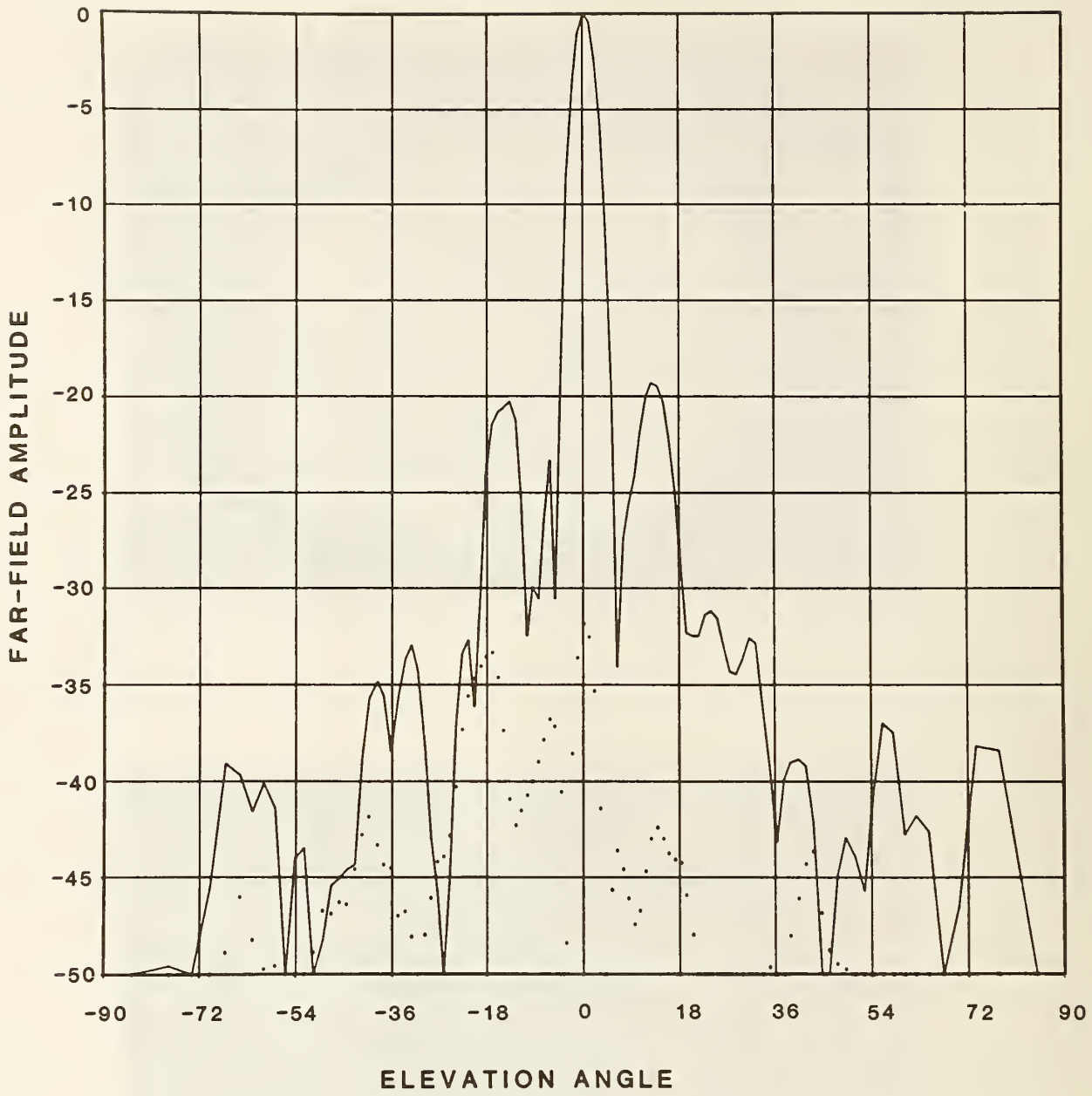

Figure 3a. Far-field radiation pattern for the reflector antenna, elevation cut. Solid curve - elevation component (parallel polarization), dotted curve - azimuth component (cross polarization).

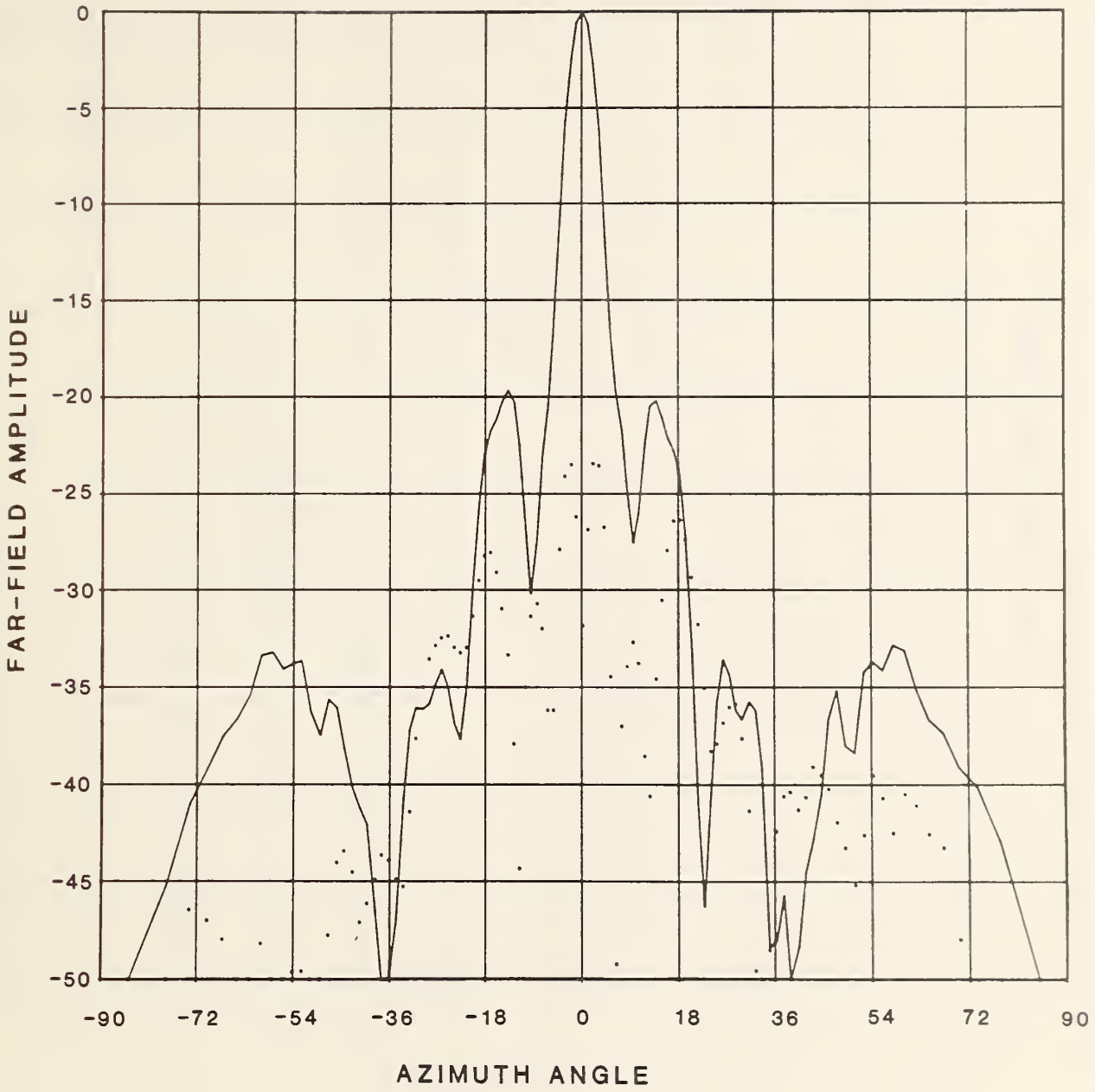

Figure 3b. Far-field radiation pattern for the reflector antenna, azimuth cut. Solid curve - elevation component (parallel polarization), dotted curve - azimuth component (cross polarization).

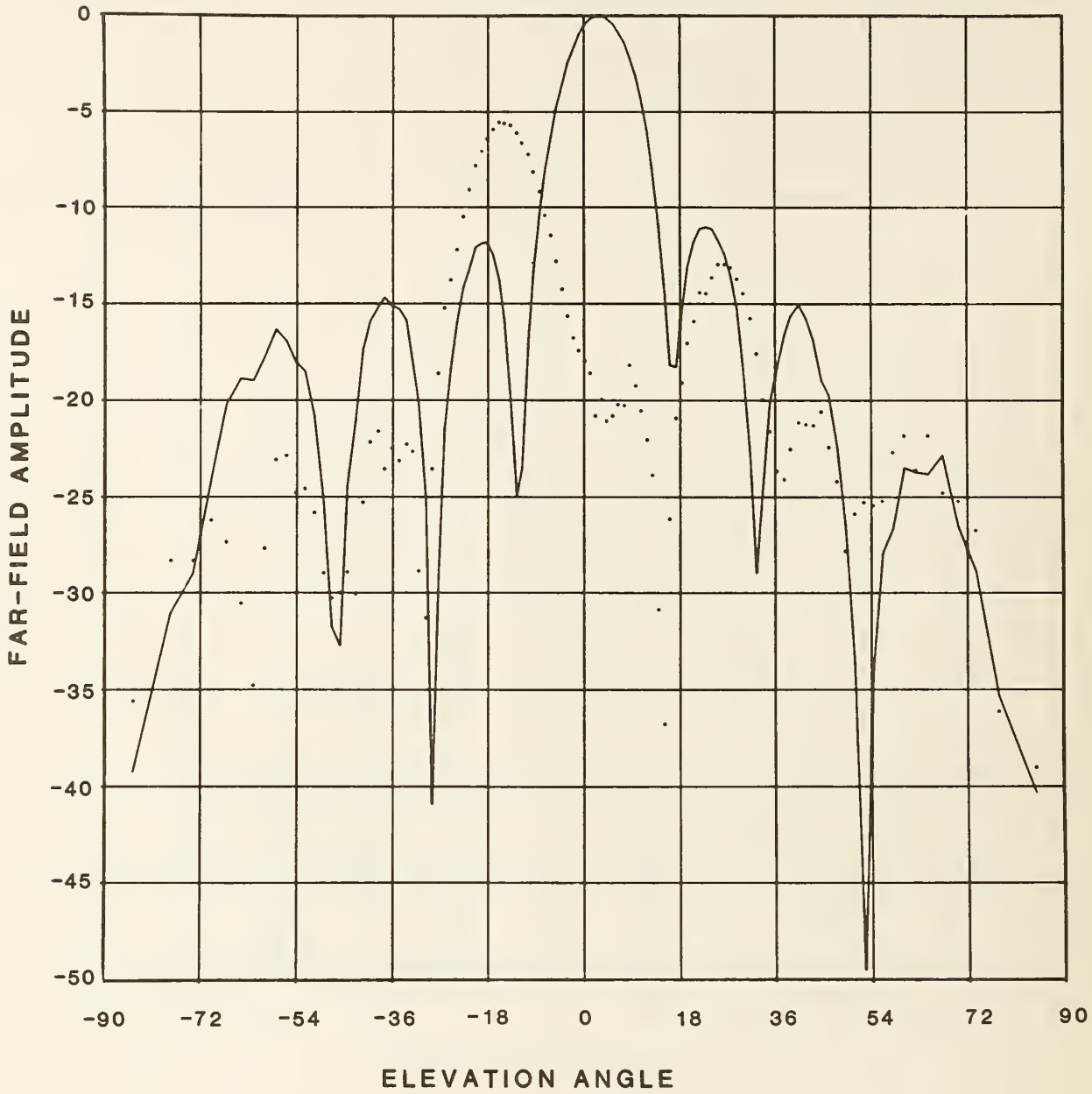

Figure 4a. Far-field radiation pattern for the microstrip array antenna, elevation cut. Solid curve - elevation component (parallel polarization), dotted curve - azimuth component (cross polarization).

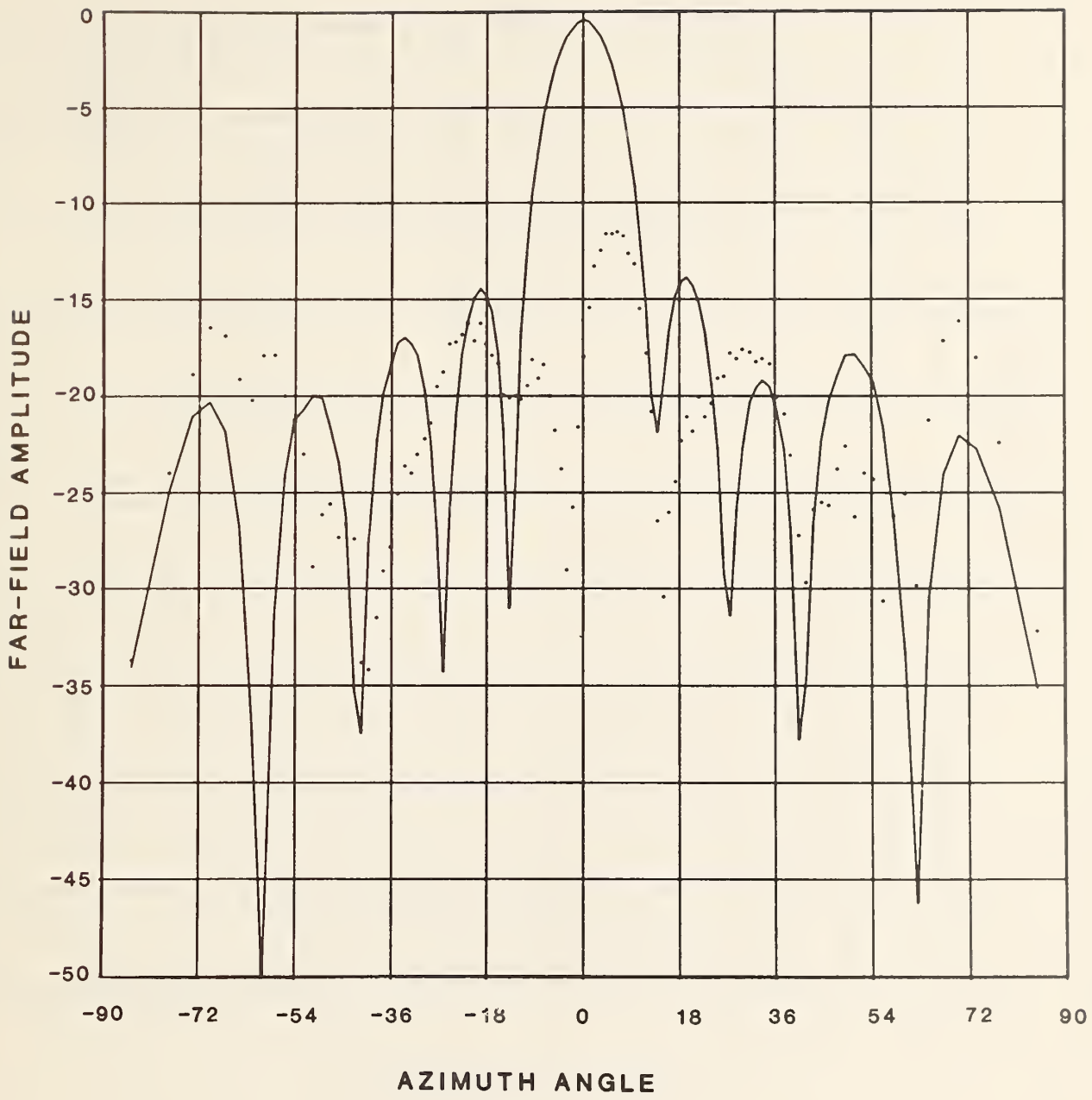

Figure 4b. Far-field radiation pattern for the microstrip array antenna, azimuth cut. Solid curve - elevation component (parallel polarization), dotted curve - azimuth component (cross polarization).

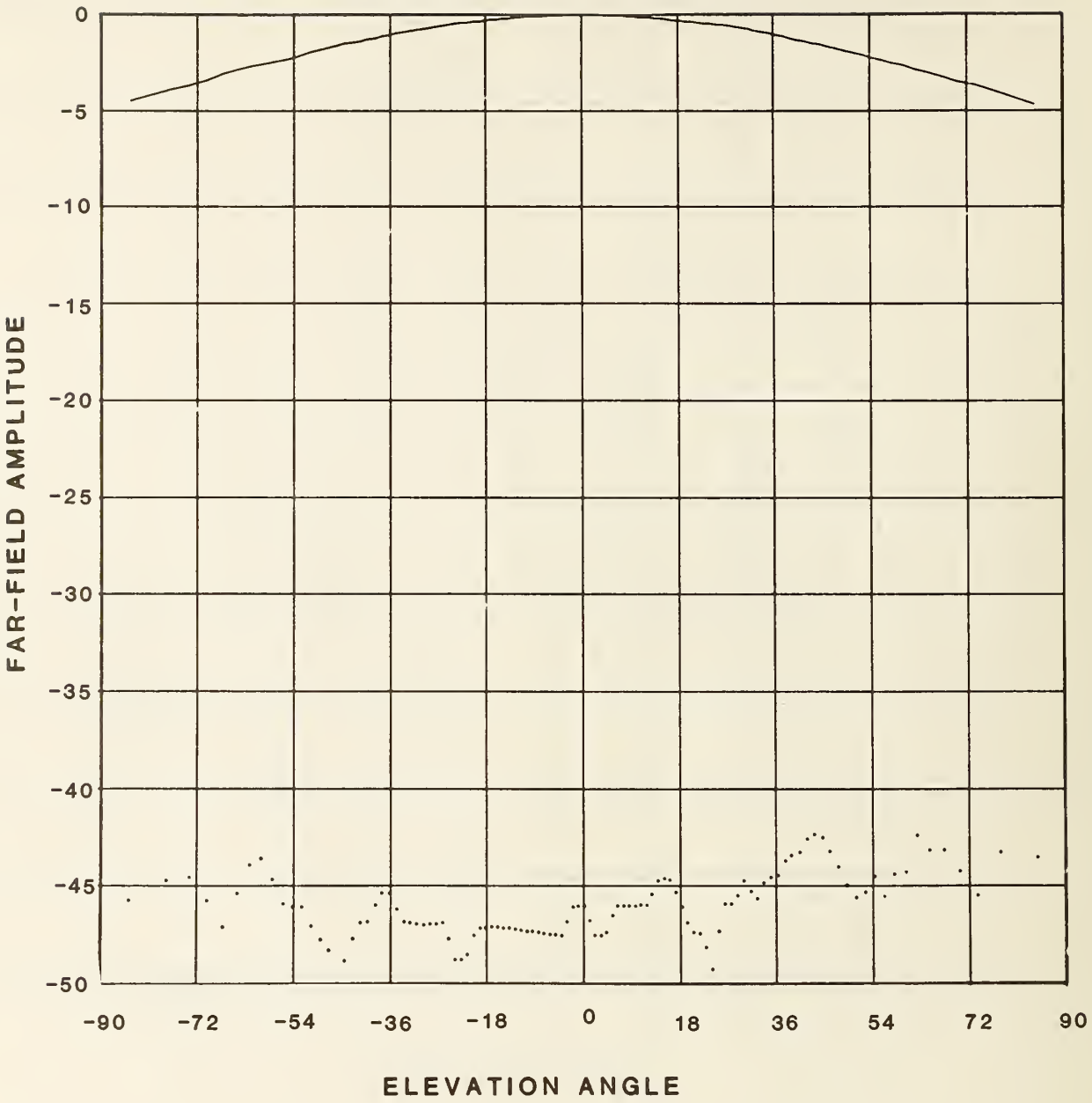

Figure 5a. Far-field radiation pattern for the open-ended waveguide antenna, elevation cut. Solid curve - elevation component (parallel polarization), dotted curve - azimuth component (cross polarization).

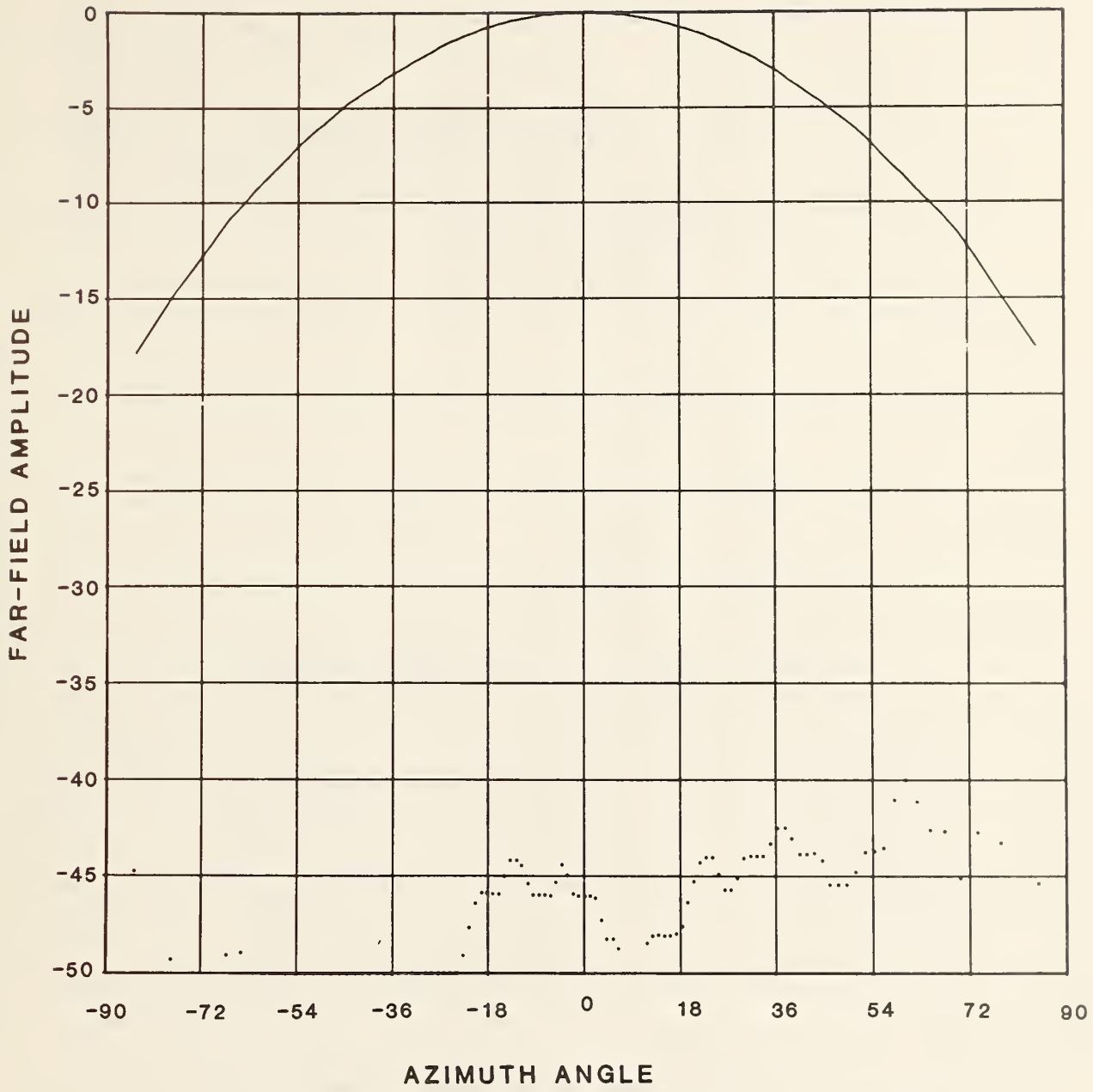

Figure 5b. Far-field radiation pattern for the open-ended waveguide antenna, azimuth cut. Solid curve - elevation component (parallel polarization), dotted curve - azimuth component (cross polarization).

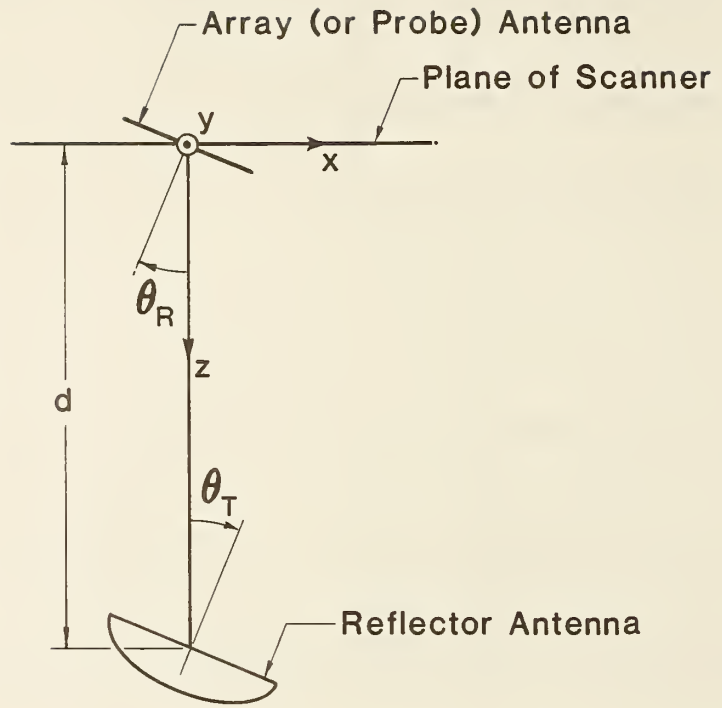

Figure 6. Definition of simplified coordinate systems for mutual coupling measurements. (See note at bottom of table I for relationship of the simplified system quantities to Eulerian angles.)

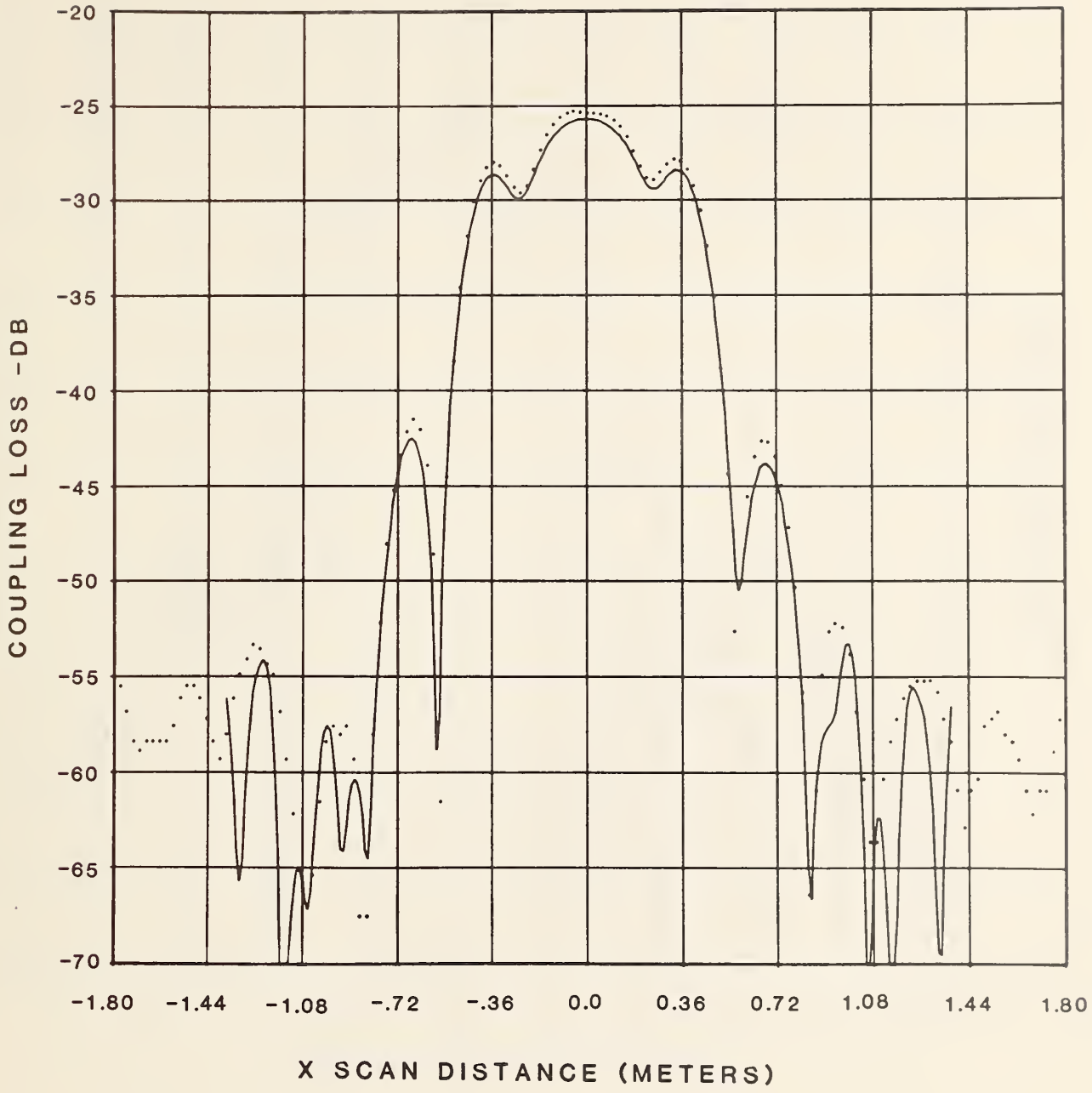

Figure 7a. Comparison of measured and calculated coupling loss between reflector and waveguide probe antennas. x-scan, $\theta_T = 0°$, $\theta_R = 0°$, d = 2.0 meters. Solid curve - calculated pattern, dotted curve - measured pattern.

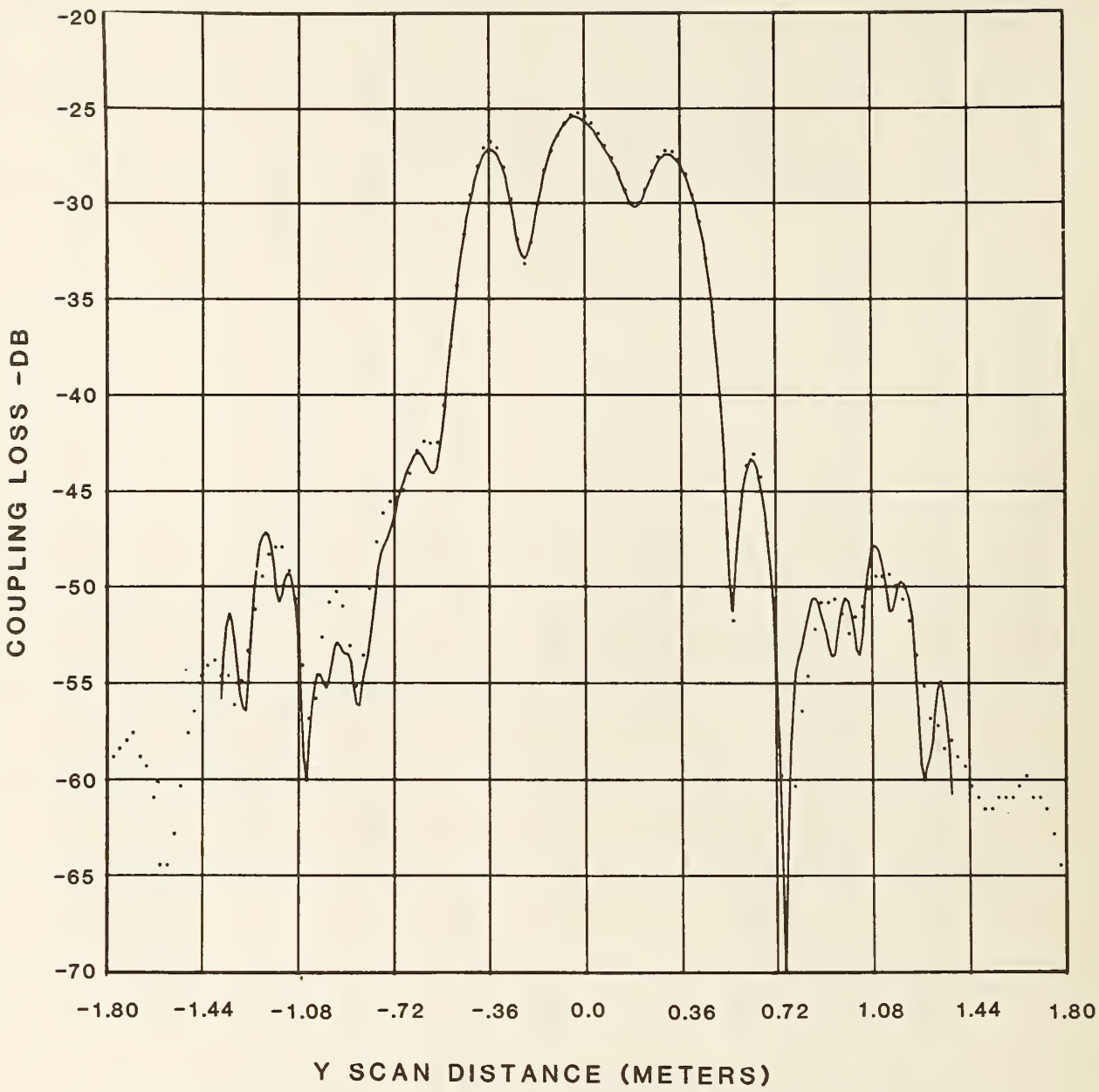

Figure 7b. Comparison of measured and calculated coupling loss between reflector and waveguide probe antennas. y-scan, $\theta_T = 0°$, $\theta_R = 0°$, d = 2.0 meters. Solid curve - calculated pattern, dotted curve - measured pattern.

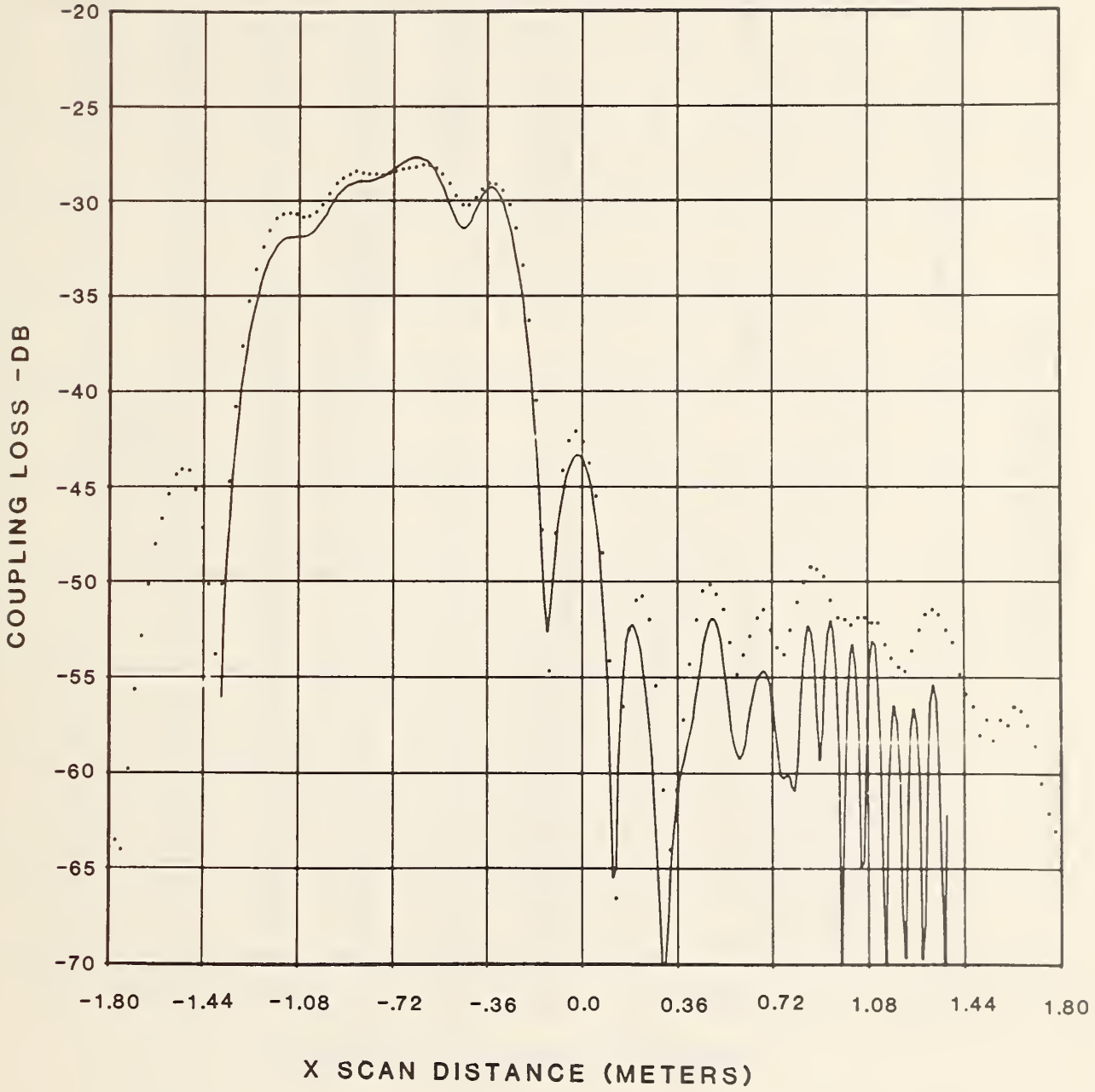

Figure 8a. Comparison of measured and calculated coupling loss between reflector and waveguide probe antennas. x-scan, $\theta_T = 20°$, $\theta_R = 0°$, d = 2.0 meters. Solid curve - calculated pattern, dotted curve - measured pattern.

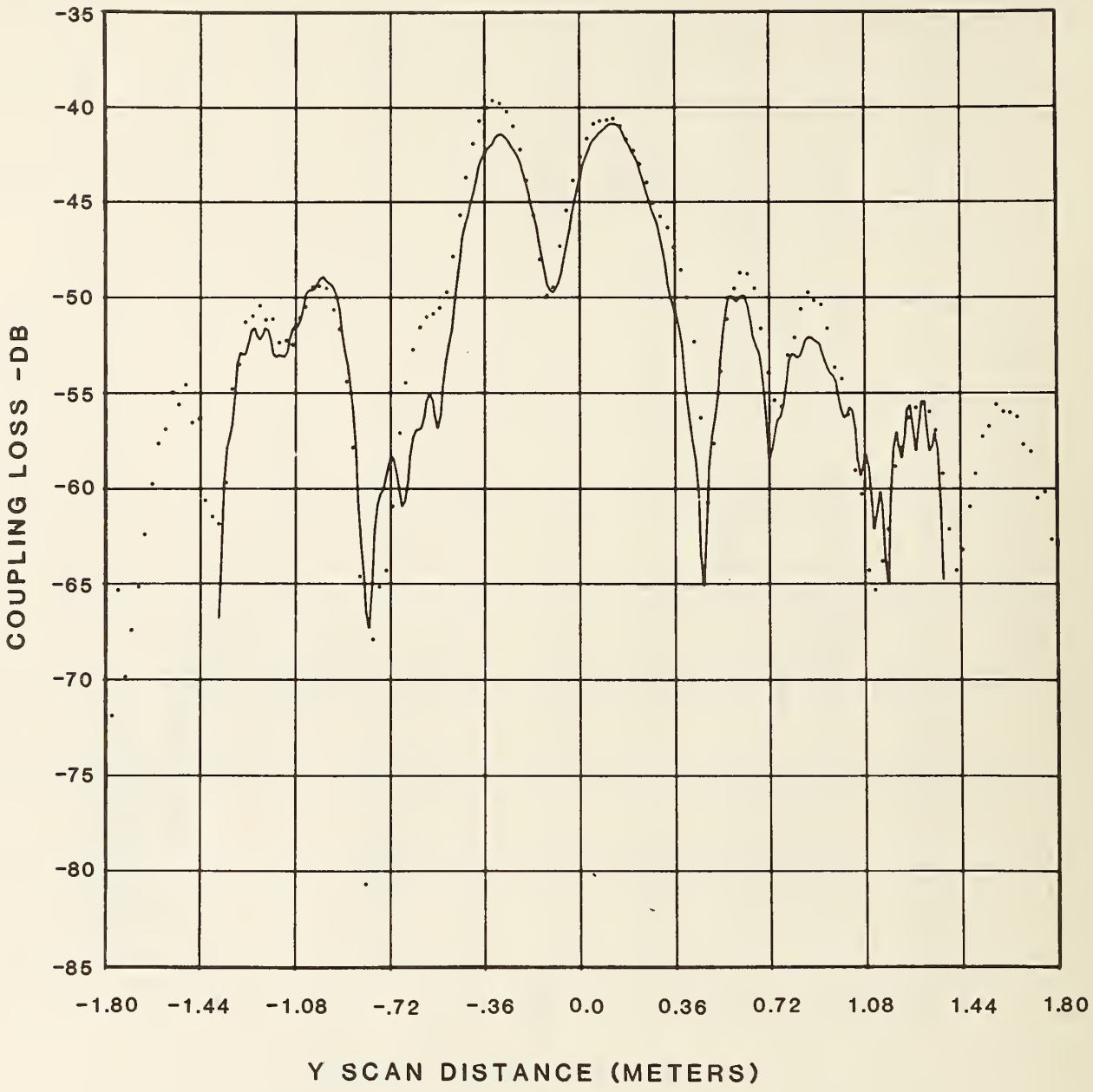

Figure 8b. Comparison of measured and calculated coupling loss between reflector and waveguide probe antennas. y-scan, $\theta_T = 20°$, $\theta_R = 0°$, d = 2.0 meters. Solid curve - calculated pattern, dotted curve - measured pattern.

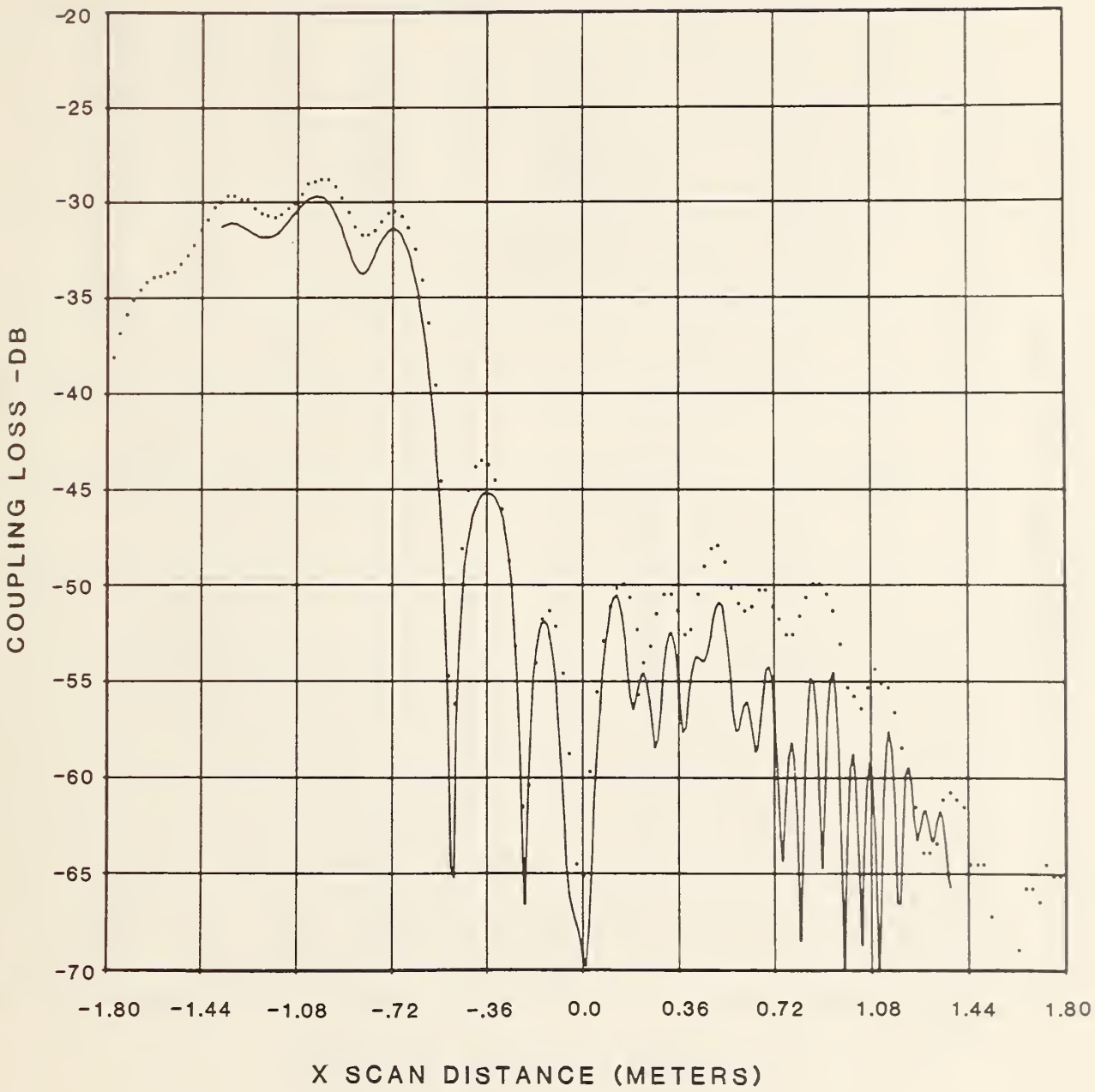

Figure 9a. Comparison of measured and calculated coupling loss between reflector and waveguide probe antennas. x-scan, $\theta_T = 30°$, $\theta_R = 0°$, d = 2.0 meters. Solid curve - calculated pattern, dotted curve - measured pattern.

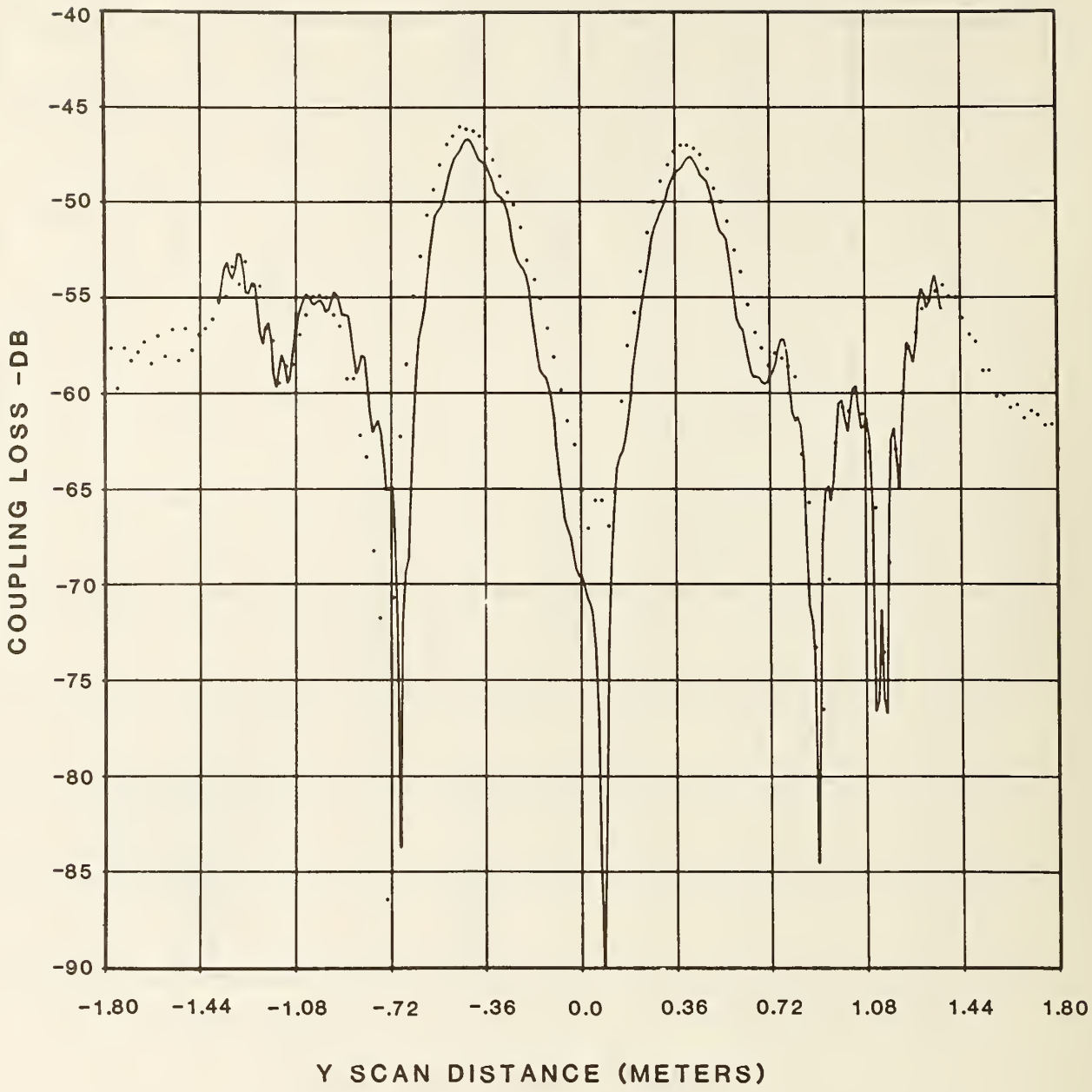

Figure 9b. Comparison of measured and calculated coupling loss between reflector and waveguide probe antennas. y-scan, $\theta_T = 30°$, $\theta_R = 0°$, d = 2.0 meters. Solid curve - calculated pattern, dotted curve - measured pattern.

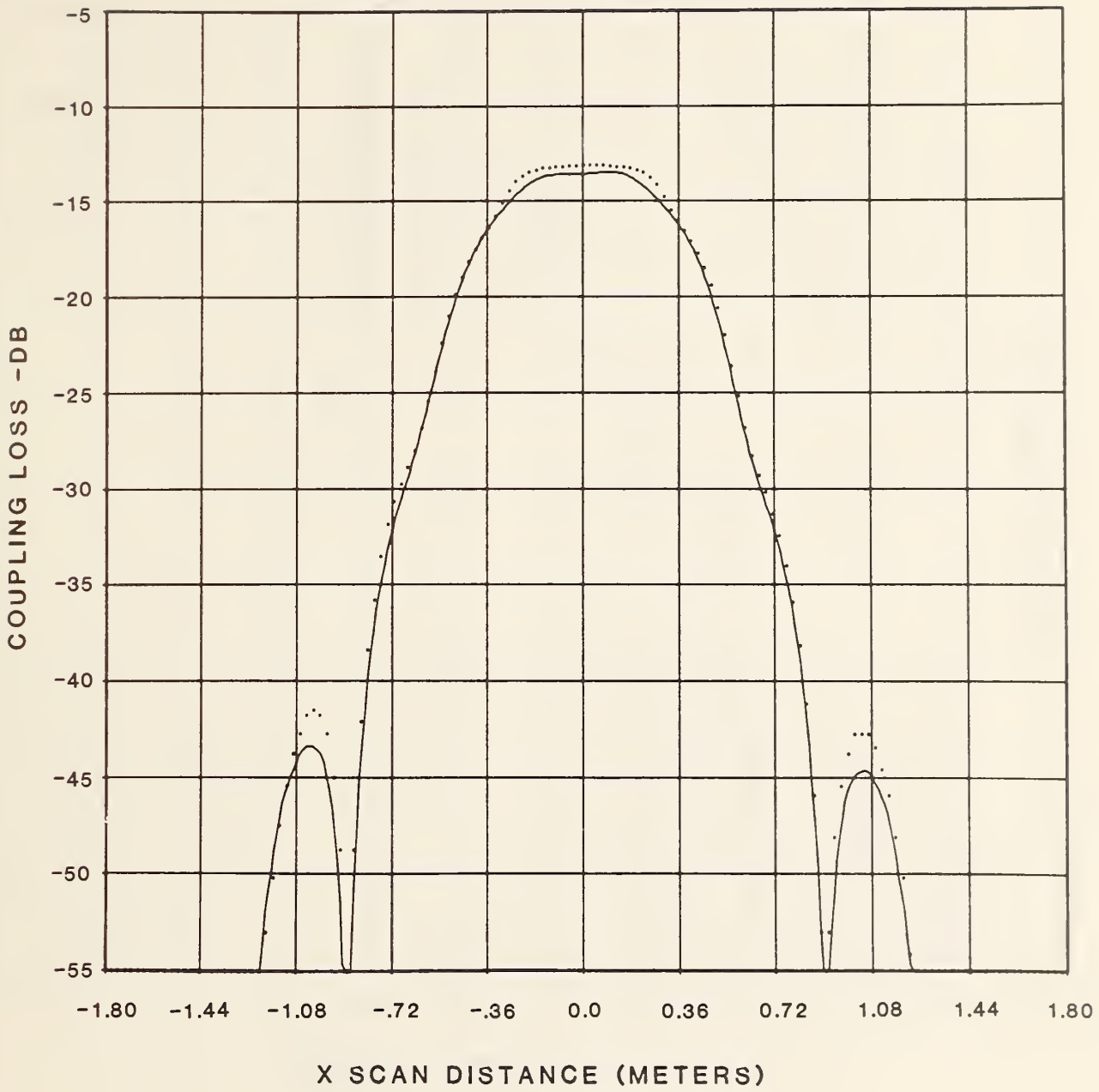

Figure 10a. Comparison of measured and calculated coupling loss between reflector and microstrip array antennas. x-scan, $\theta_T = 0°$, $\theta_R = 0°$, $d = 3.0$ meters. Solid curve - calculated pattern, dotted curve - measured pattern.

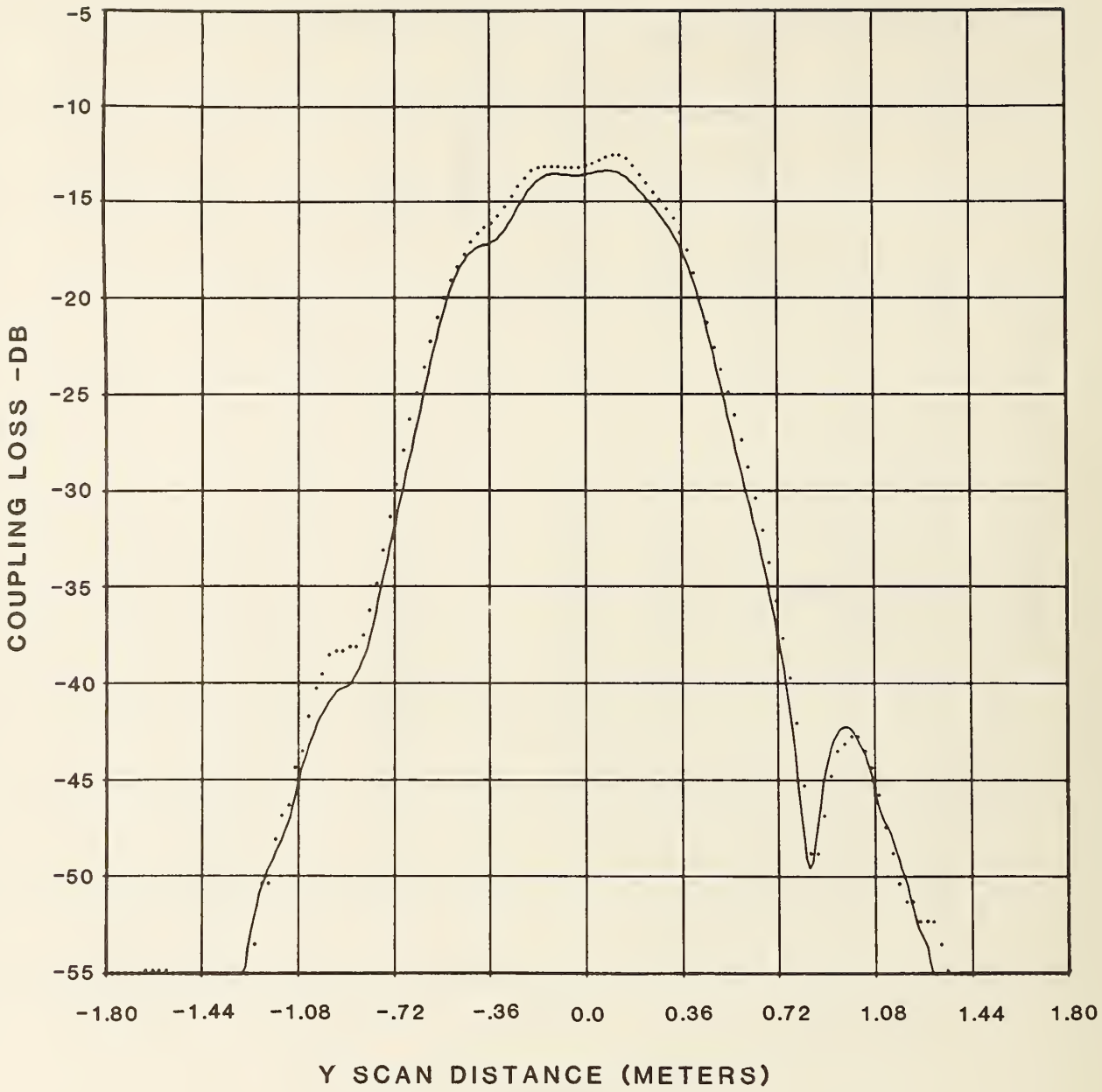

Figure 10b. Comparison of measured and calculated coupling loss between reflector and microstrip array antennas. y-scan, $\theta_T = 0°$, $\theta_R = 0°$, d = 3.0 meters. Solid curve - calculated pattern, dotted curve - measured pattern.

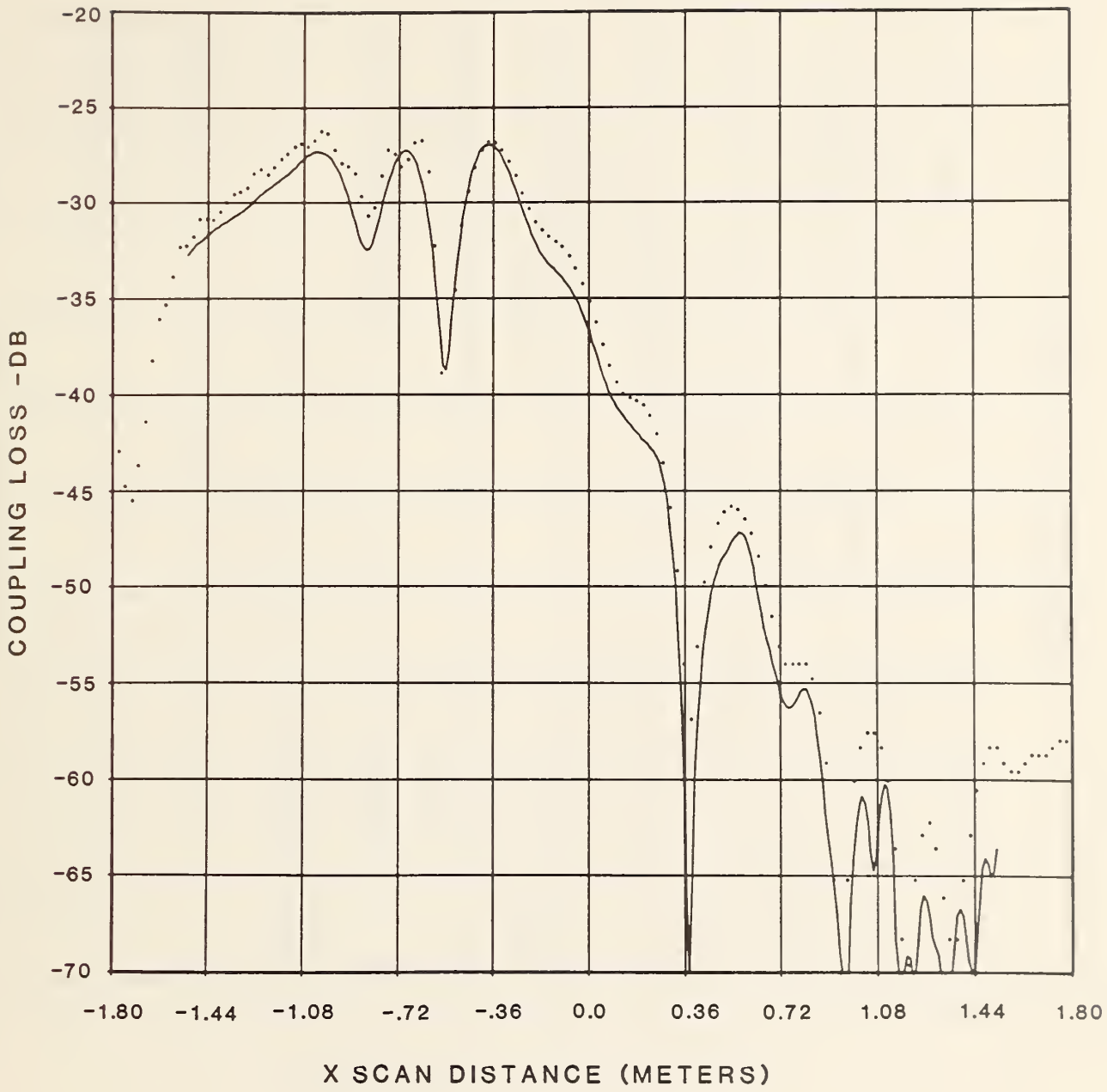

Figure 11a. Comparison of measured and calculated coupling loss between reflector and microstrip array antennas. x-scan, $\theta_T = 20°$, $\theta_R = 0°$, d = 3.0 meters. Solid curve - calculated pattern, dotted curve - measured pattern.

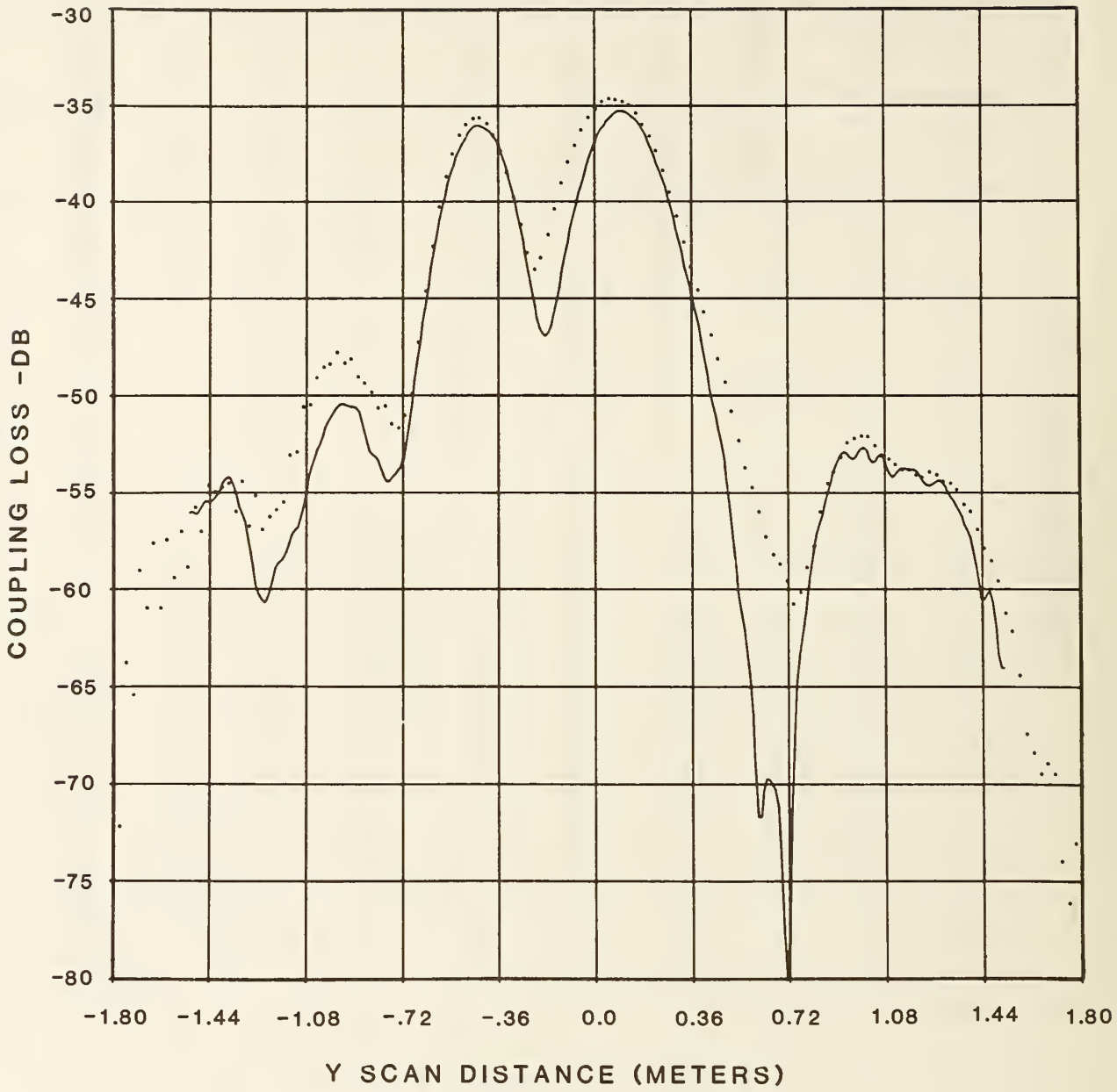

Figure 11b. Comparison of measured and calculated coupling loss between reflector and microstrip array antennas. y-scan, θ_T = 20°, θ_R = 0°, d = 3.0 meters. Solid curve - calculated pattern, dotted curve - measured pattern.

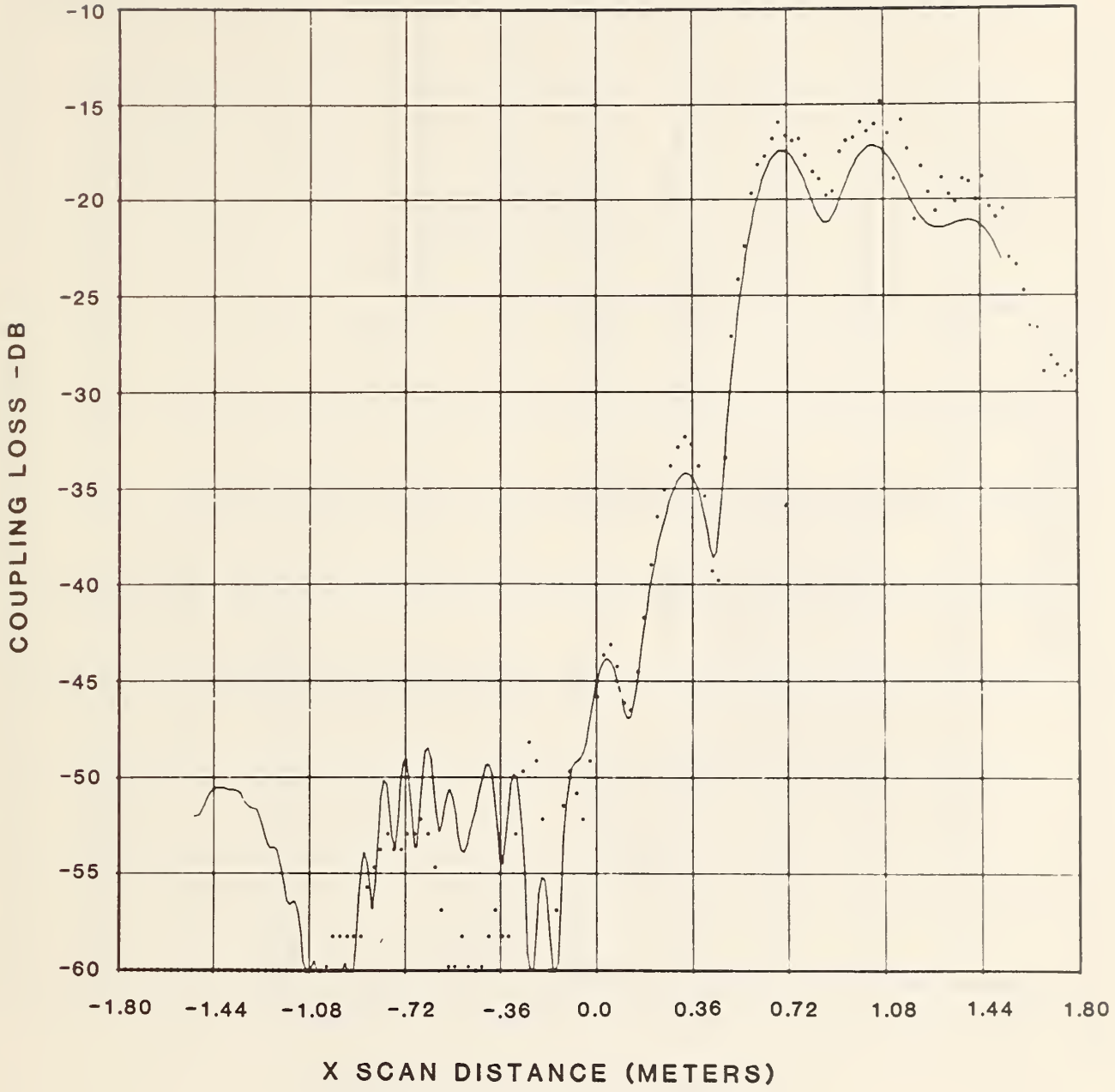

Figure 12a. Comparison of measured and calculated coupling loss between reflector and microstrip array antennas. x-scan, θ_T = -30°, θ_R = -21.6°. d = 2.0 meters. Solid curve - calculated pattern, dotted curve - measured pattern.

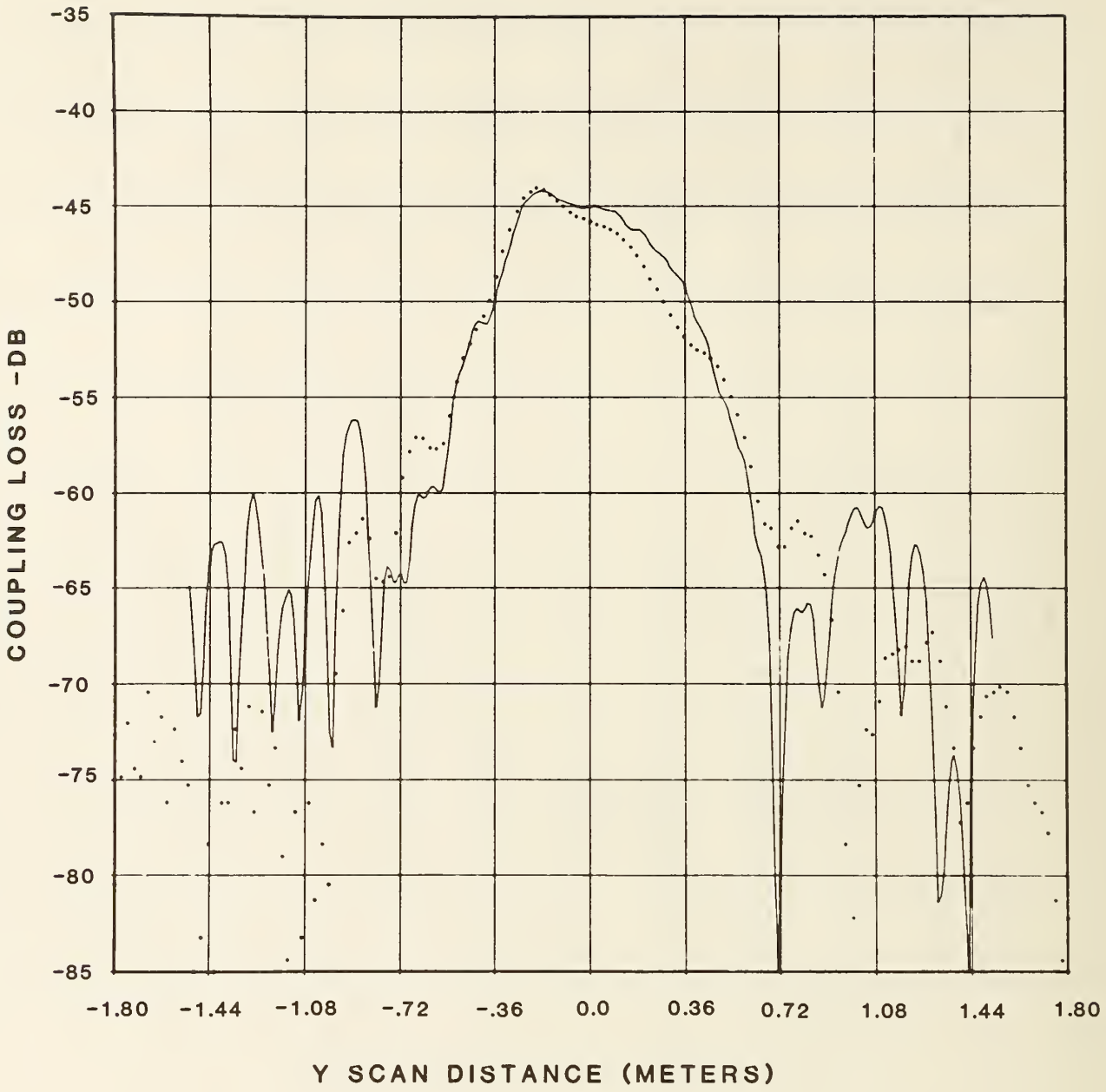

Figure 12b. Comparison of measured and calculated coupling loss between reflector and microstrip array antennas. y-scan, θ_T = -30°, θ_R = -21.6°, d = 2.0 meters. Solid curve - calculated pattern, dotted curve - measured pattern.

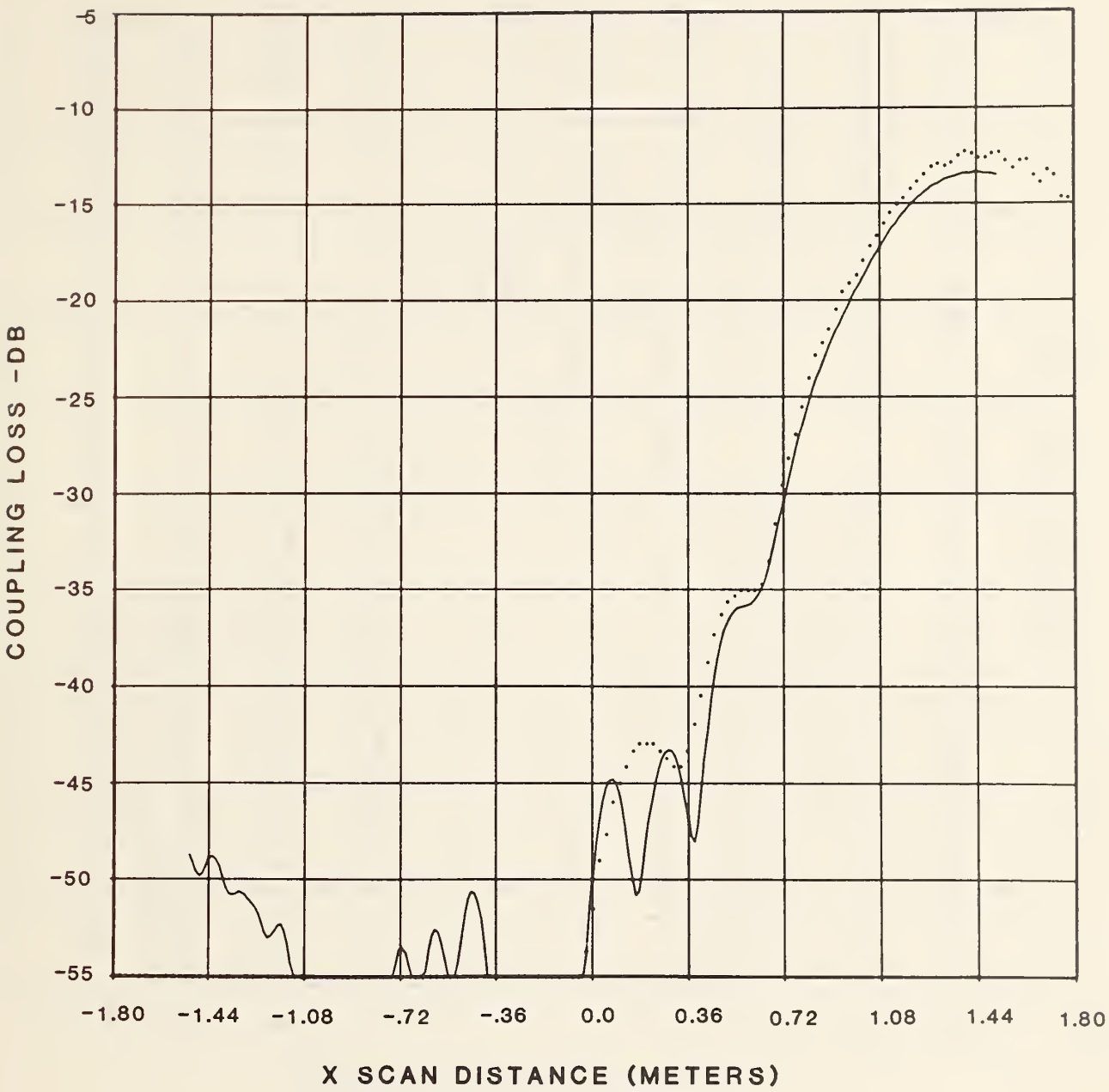

Figure 13a. Comparison of measured and calculated coupling loss between reflector and microstrip array antennas. x-scan, θ_T = -20°, θ_R = -21.6°, d = 4.0 meters. Solid curve - calculated pattern, dotted curve - measured pattern.

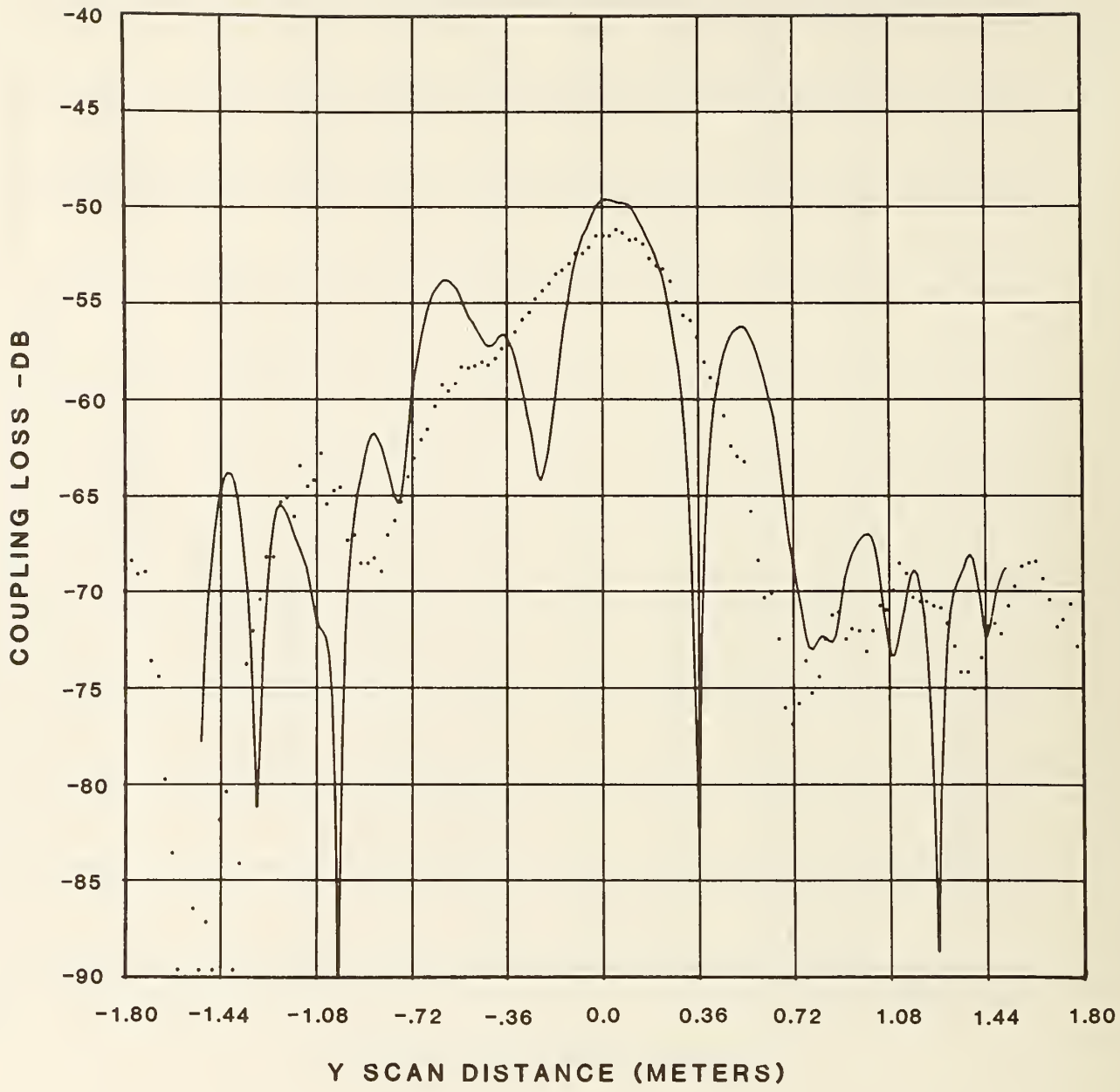

Figure 13b. Comparison of measured and calculated coupling loss between reflector and microstrip array antennas. y-scan, θ_T = -20°, θ_R = -21.6°, d = 4.0 meters. Solid curve - calculated pattern, dotted curve - measured pattern.

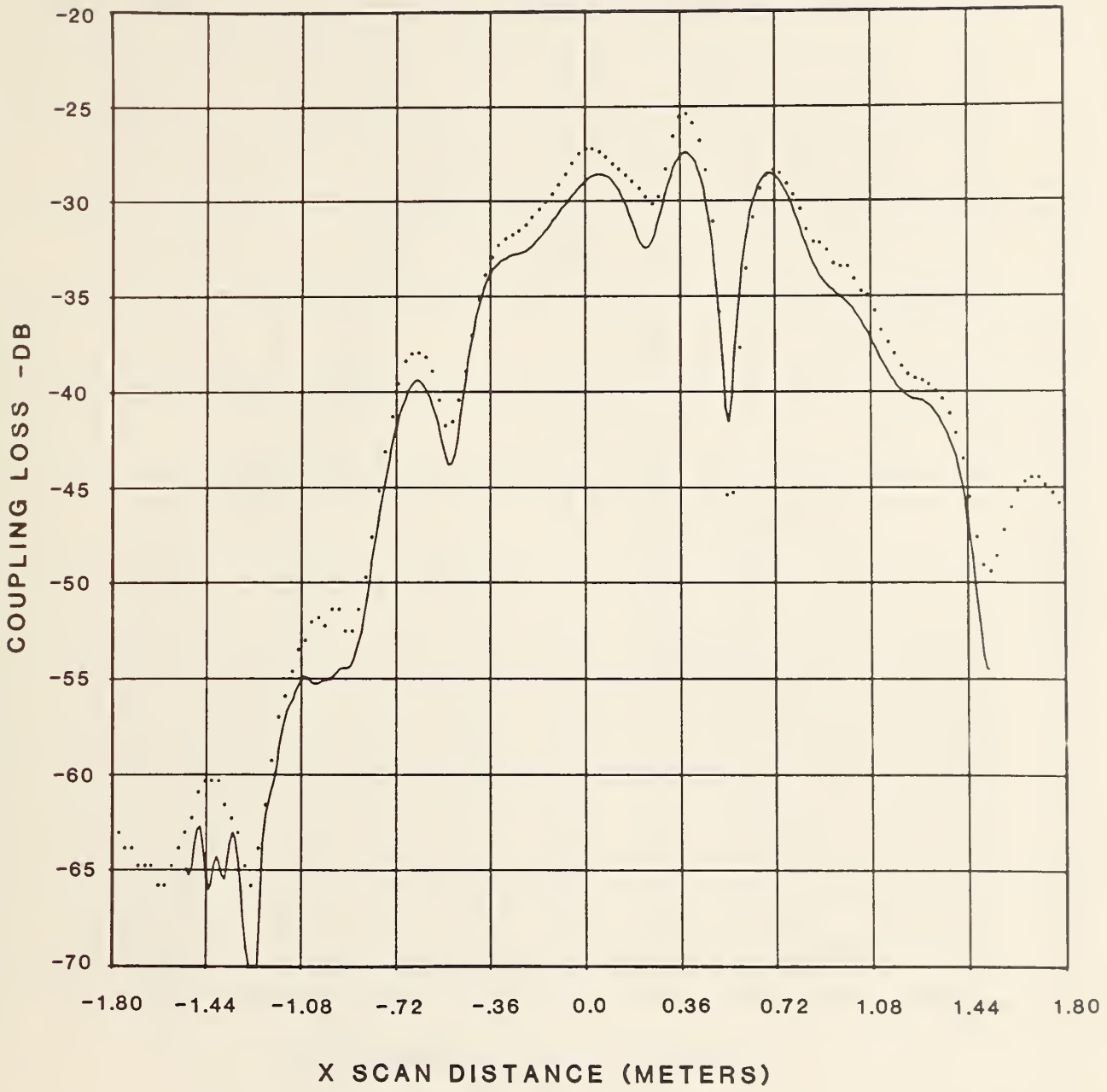

Figure 14a. Comparison of measured and calculated coupling loss between reflector and microstrip array antennas. x-scan, $\theta_T = 0°$, $\theta_R = -21.6°$, d = 3.0 meters. Solid curve - calculated pattern, dotted curve - measured pattern.

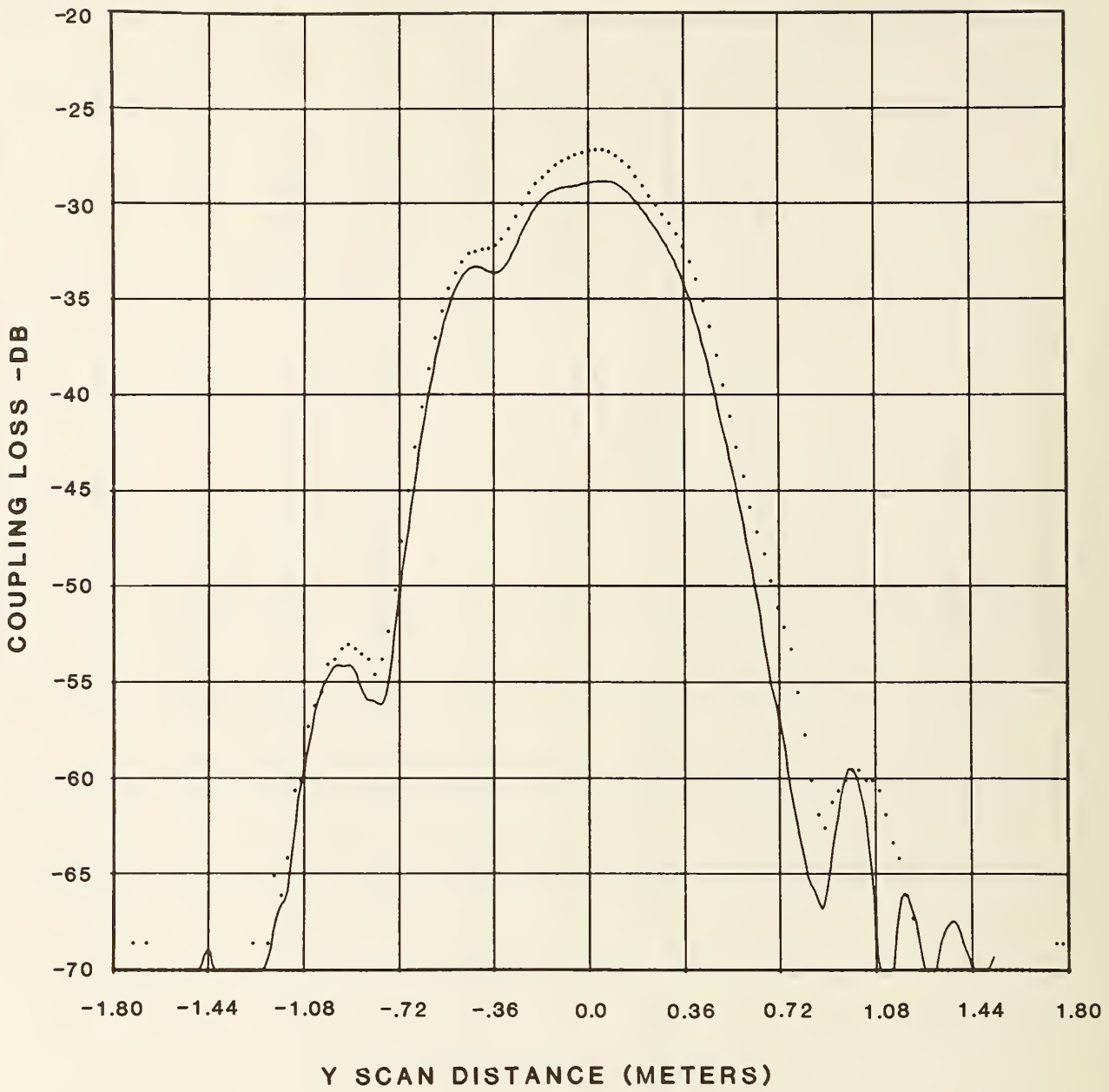

Figure 14b. Comparison of measured and calculated coupling loss between reflector and microstrip array antennas. y-scan, θ_T = 0°, θ_R = -21.6°, d = 3.0 meters. Solid curve - calculated pattern, dotted curve - measured pattern.

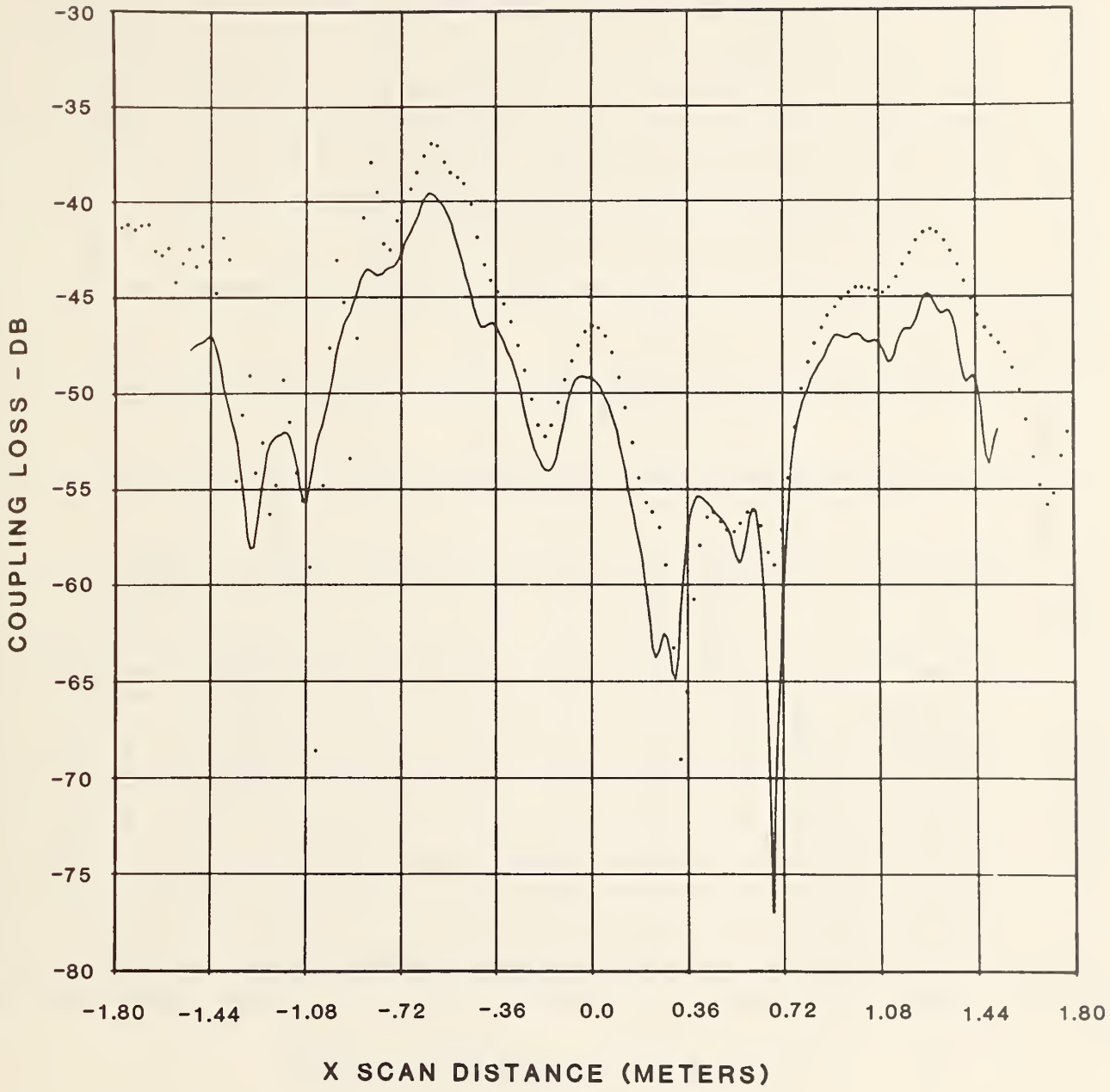

Figure 15a. Comparison of measured and calculated coupling loss between reflector and microstrip array antennas. x-scan, θ_T = 20°, θ_R = -21.6°, d = 3.0 meters. Solid curve - calculated pattern, dotted curve - measured pattern.

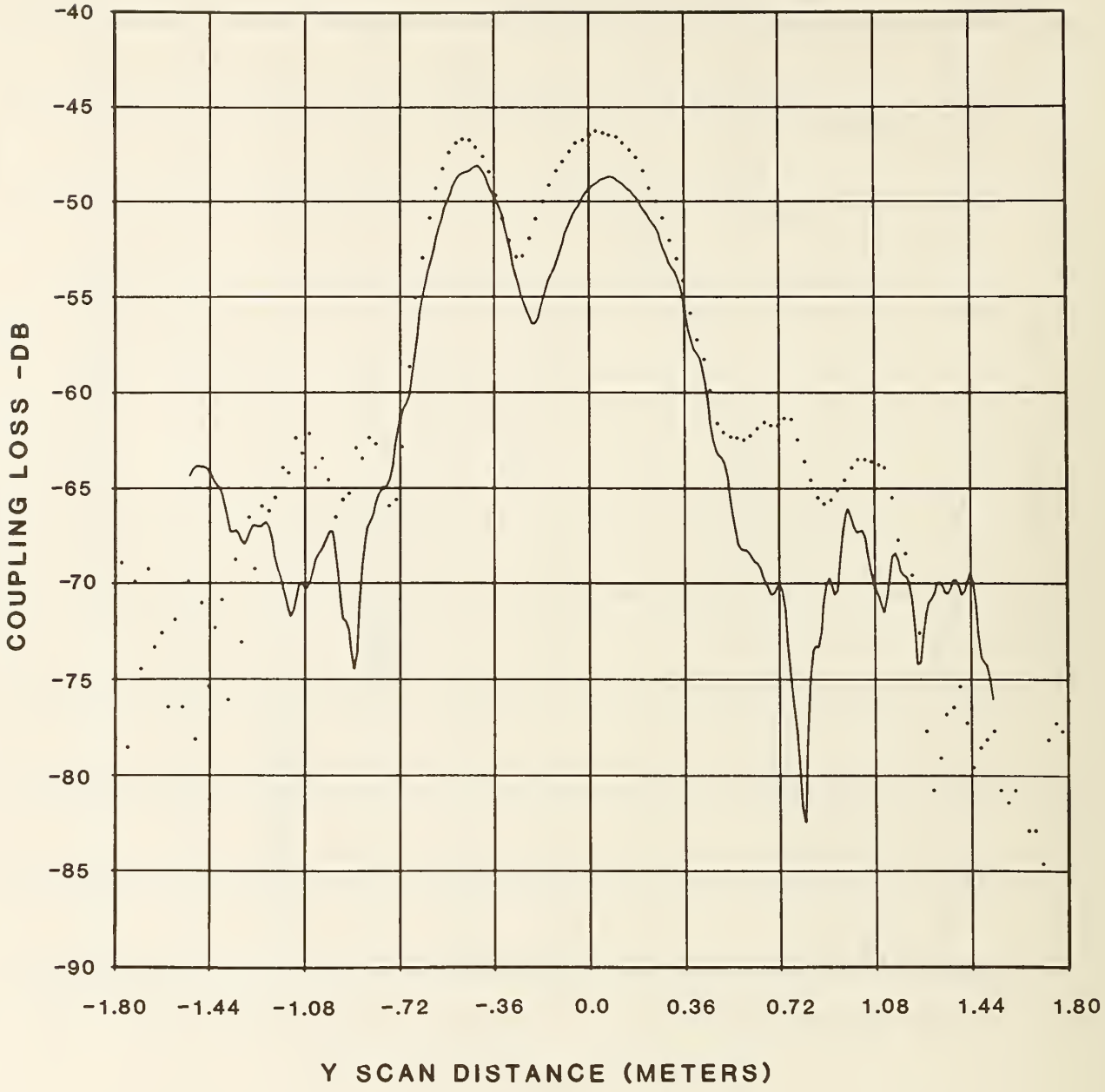

Figure 15b. Comparison of measured and calculated coupling loss between reflector and microstrip array antennas. y-scan, θ_T = 20°, θ_R = -21.6°, d = 3.0 meters. Solid curve - calculated pattern, dotted curve - measured pattern.

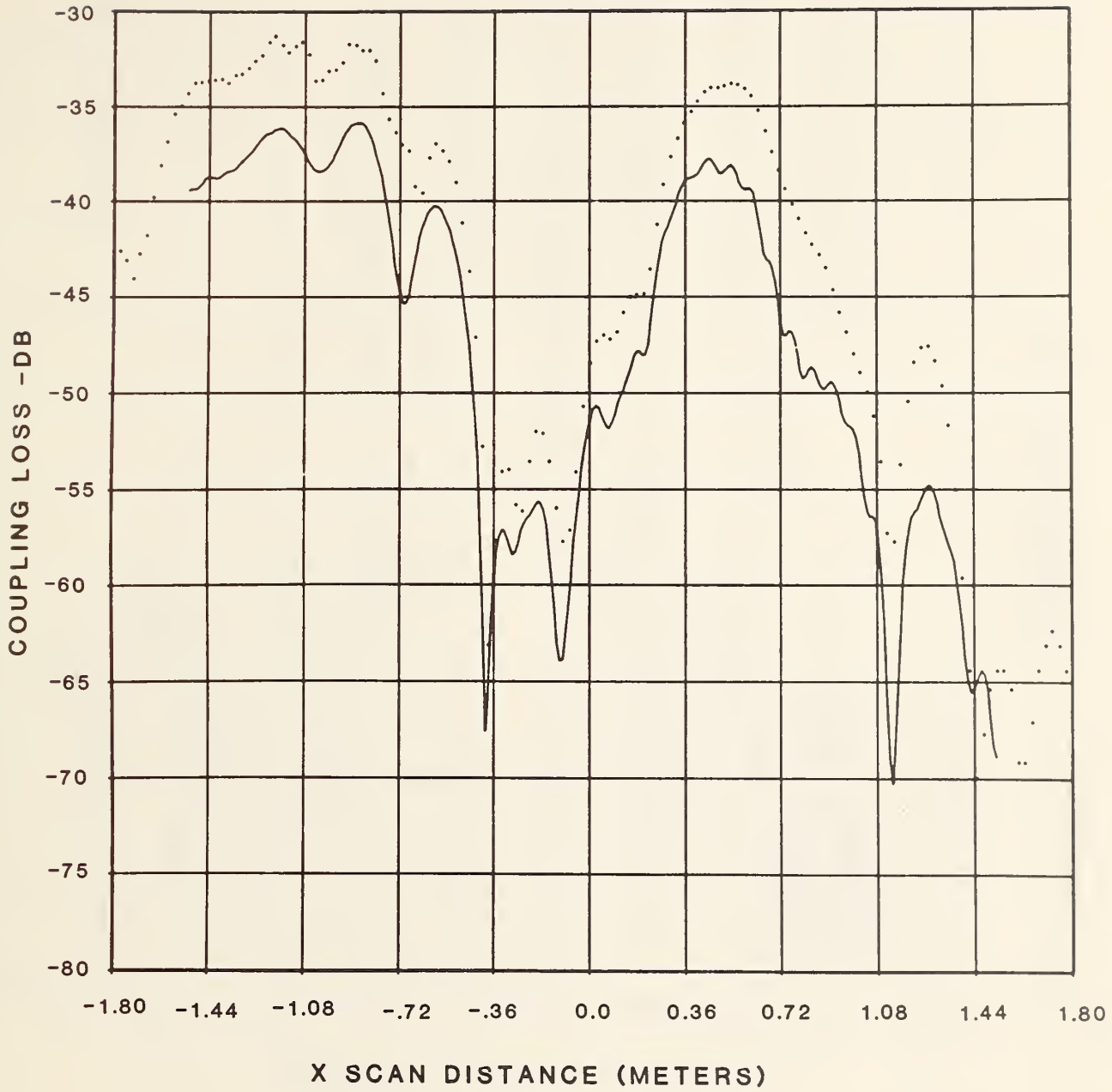

Figure 16a. Comparison of measured and calculated coupling loss between reflector and microstrip array antennas. x-scan, θ_T = 30°, θ_R = -21.6°, d = 2.0 meters. Solid curve - calculated pattern, dotted curve - measured pattern.

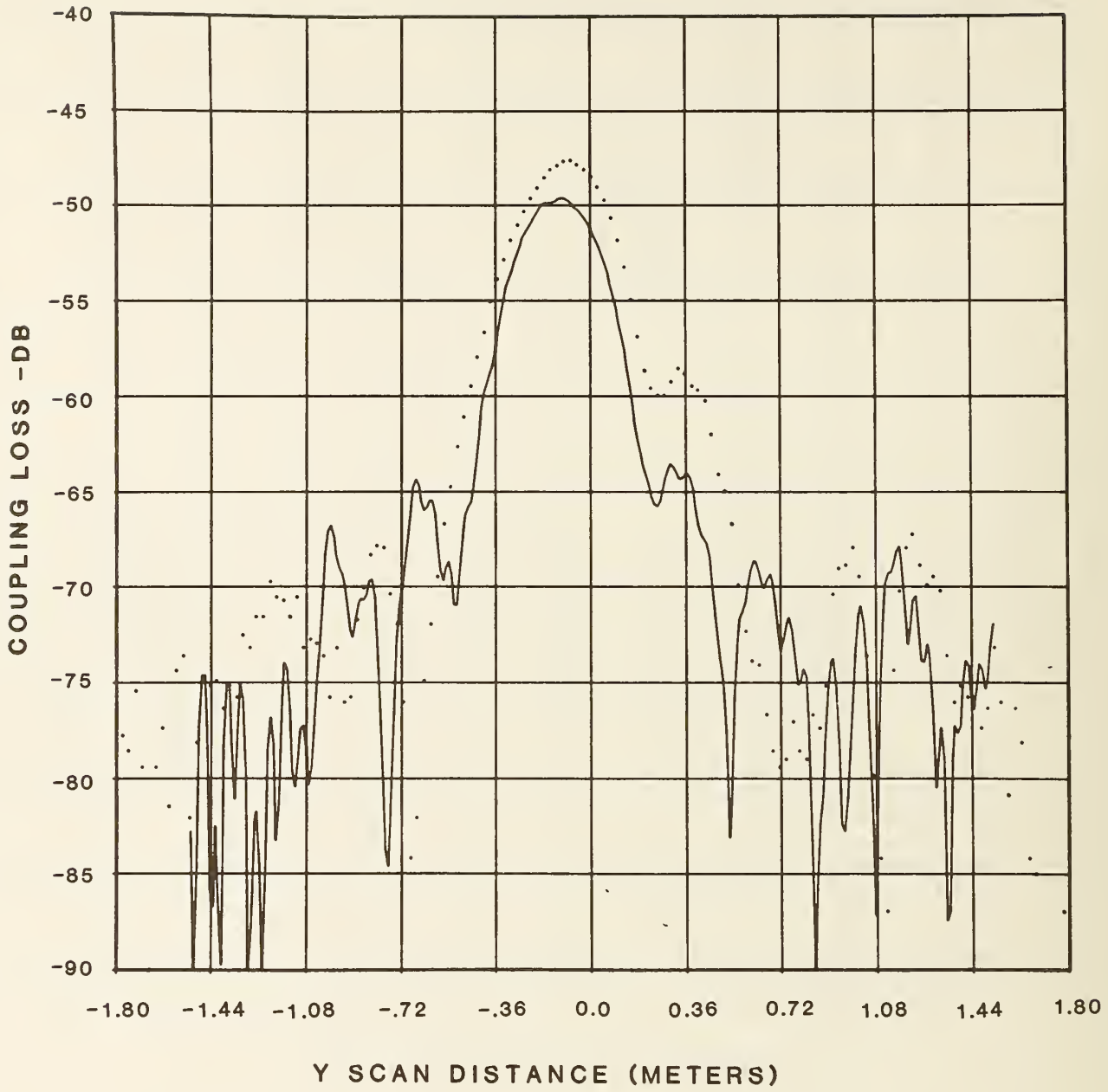

Figure 16b. Comparison of measured and calculated coupling loss between reflector and microstrip array antennas. y-scan, θ_T = 30°, θ_R = -21.6°, d = 2.0 meters. Solid curve - calculated pattern, dotted curve - measured pattern.

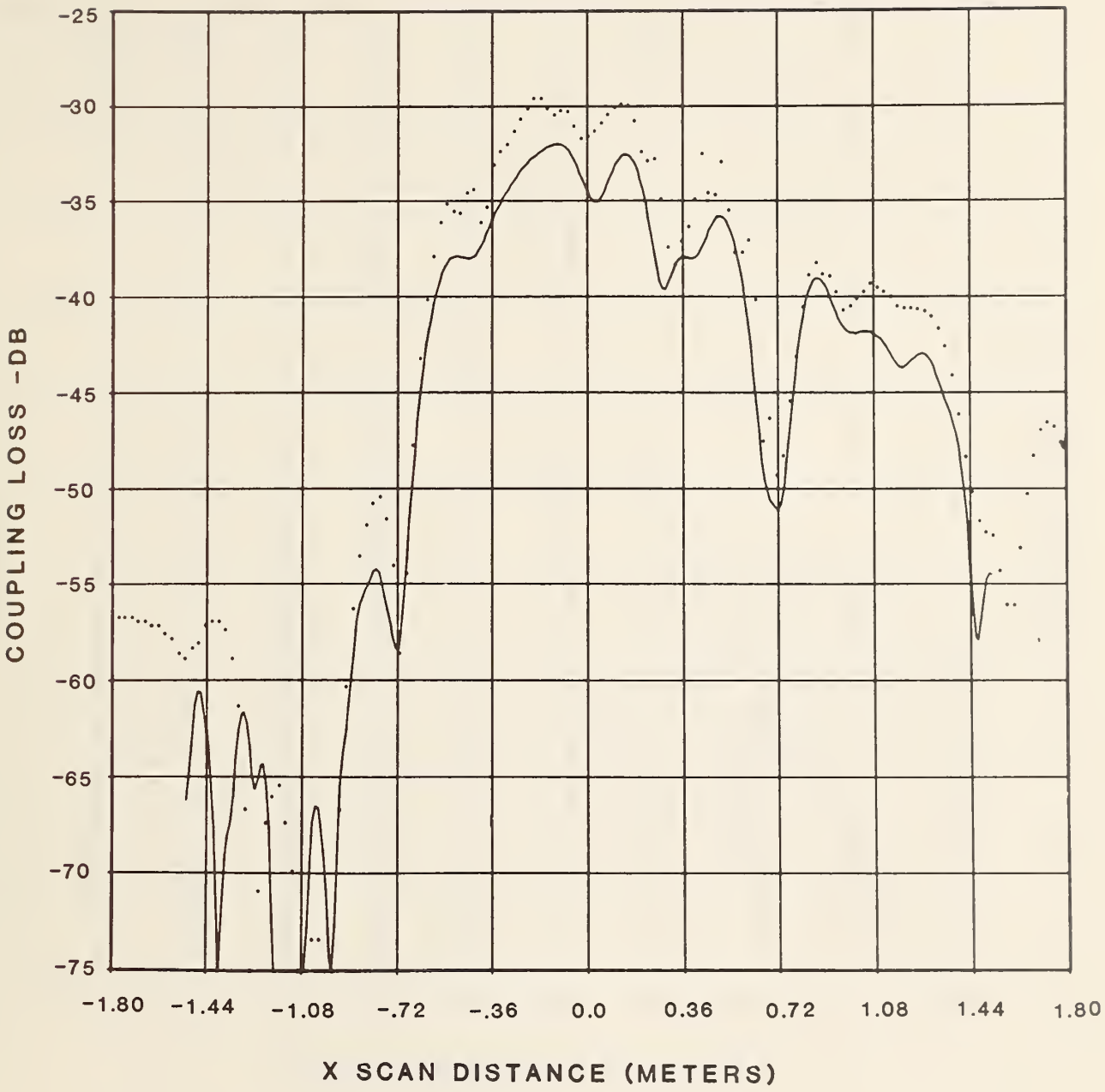

Figure 17a. Comparison of measured and calculated coupling loss between reflector and microstrip array antennas. x-scan, θ_T = 0°, θ_R = -30.3°, d = 2.0 meters. Solid curve - calculated pattern, dotted curve - measured pattern.

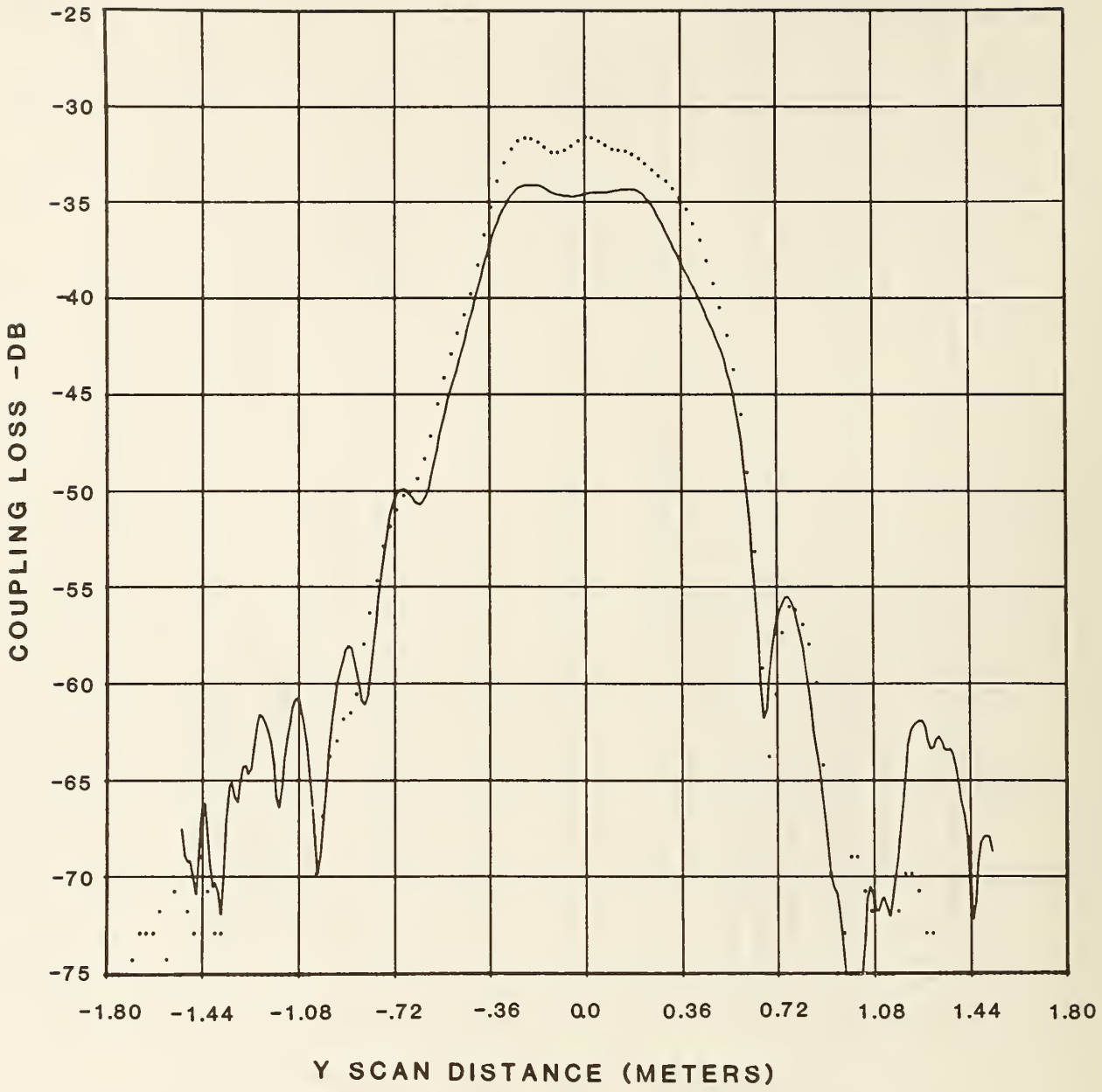

Figure 17b. Comparison of measured and calculated coupling loss between reflector and microstrip array antennas. y-scan, θ_T = 0°, θ_R = -30.3°, d = 2.0 meters. Solid curve - calculated pattern, dotted curve - measured pattern.

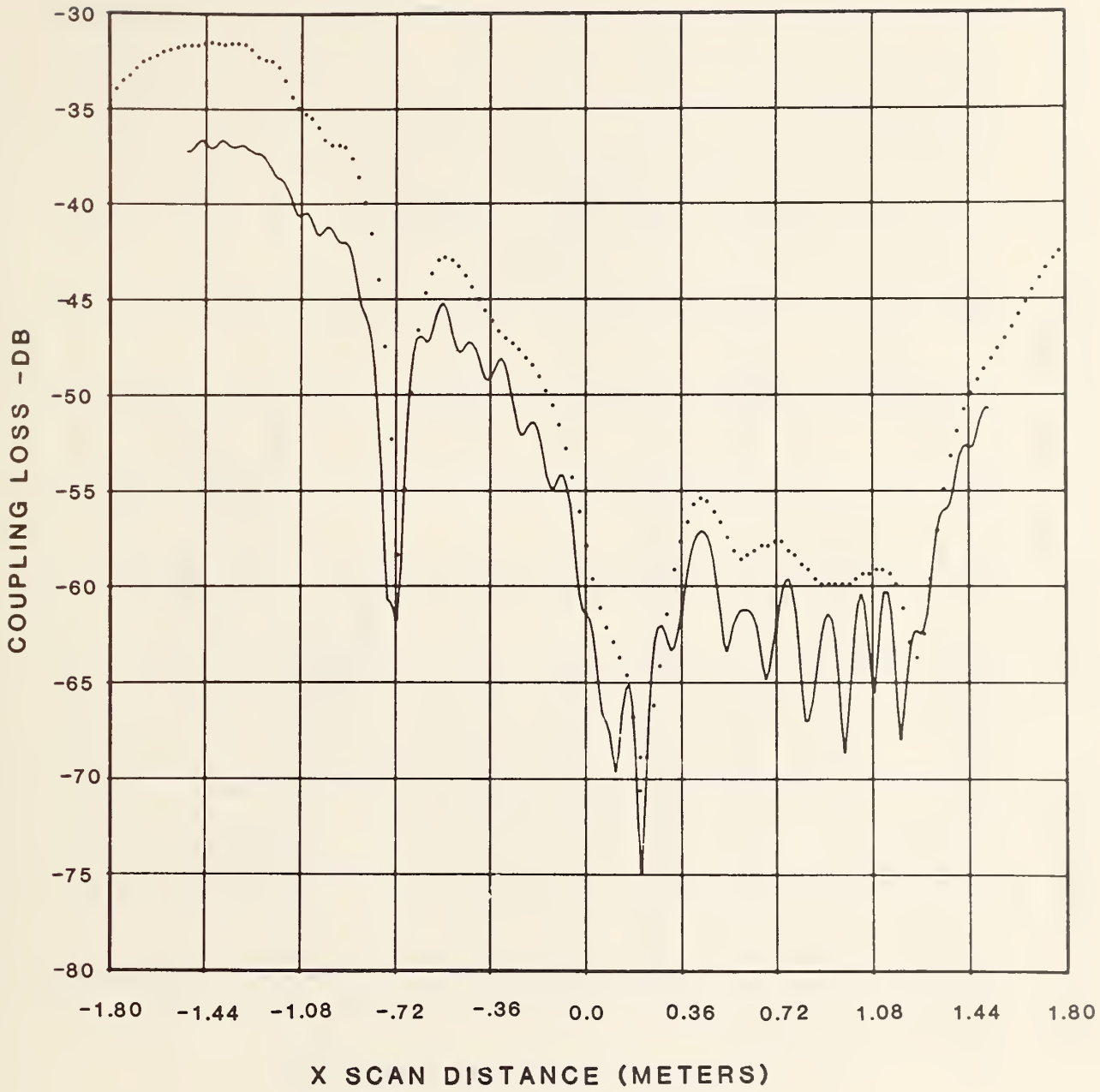

Figure 18a. Comparison of measured and calculated coupling loss between reflector and microstrip array antennas. x-scan, θ_T = 20°, θ_R = -30.3°, d = 4.0 meters. Solid curve - calculated pattern, dotted curve - measured pattern.

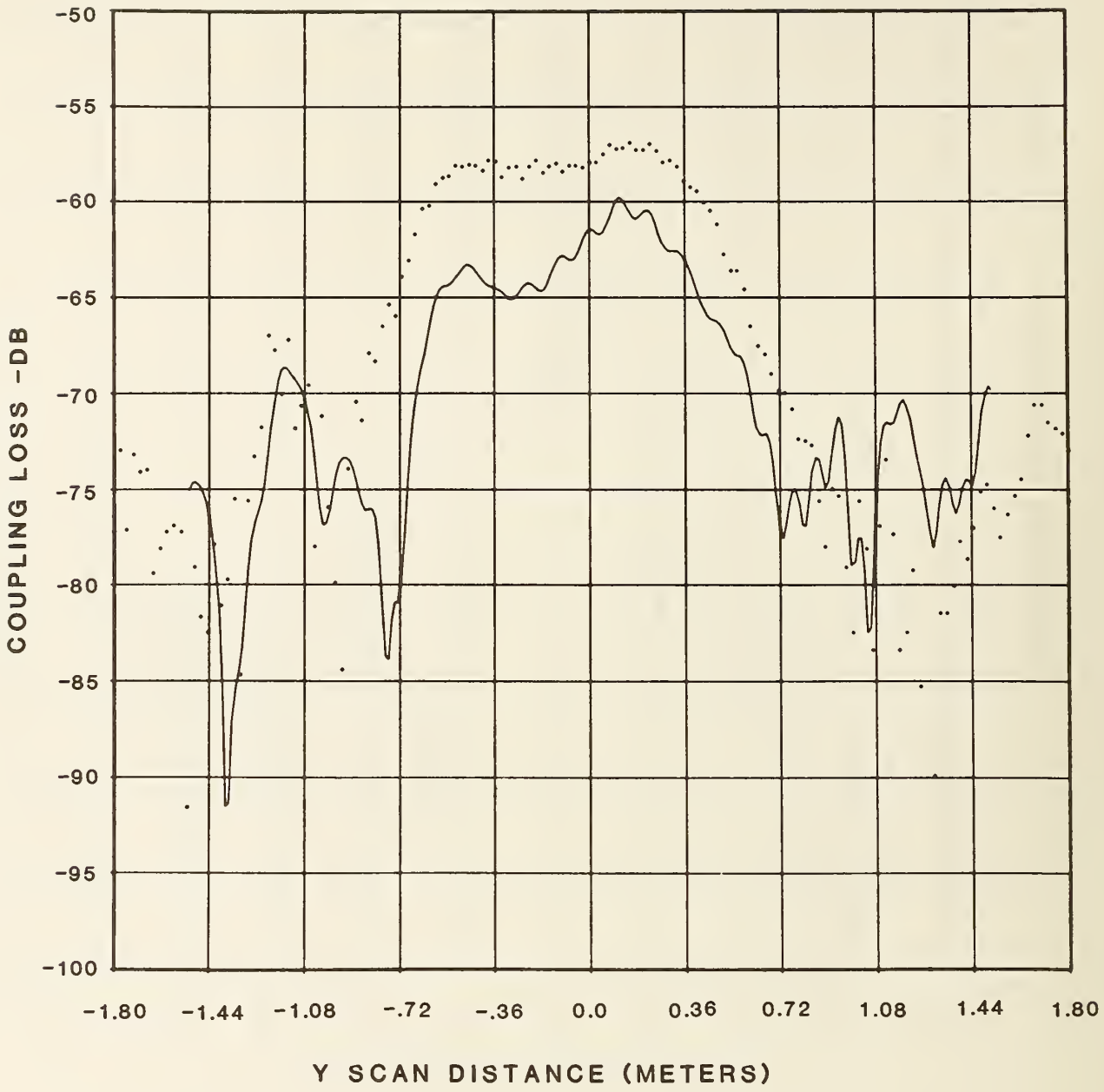

Figure 18b. Comparison of measured and calculated coupling loss between reflector and microstrip array antennas. y-scan, θ_T = 20°, θ_R = -30.3°, d = 4.0 meters. Solid curve - calculated pattern, dotted curve - measured pattern.

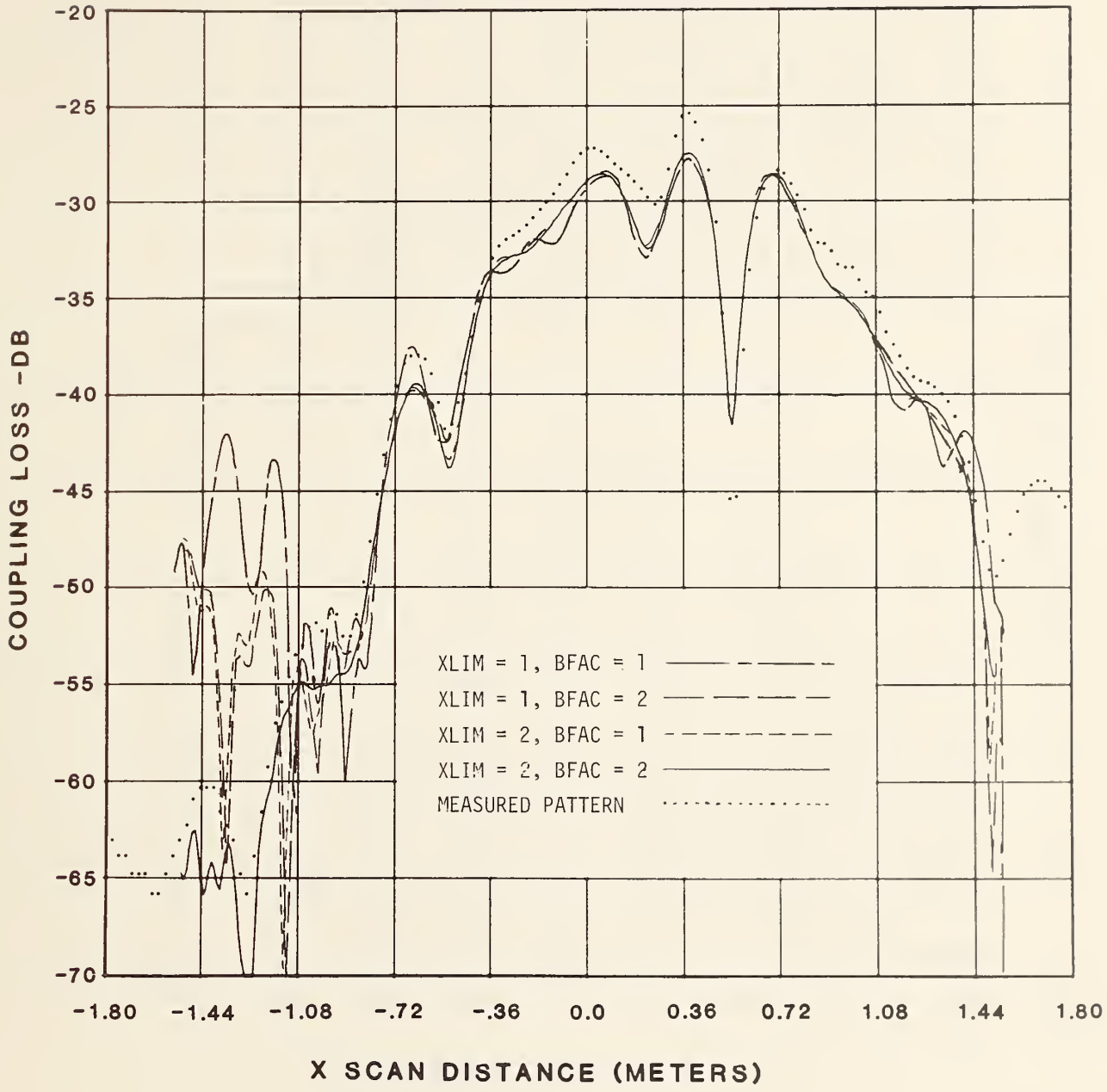

Figure 19. Comparison of coupling losses calculated using various values of the parameters XLIM and BFAC to measured losses. x-scan, $\theta_T = 0°$, $\theta_R = -21.6°$, d = 3.0 meters.

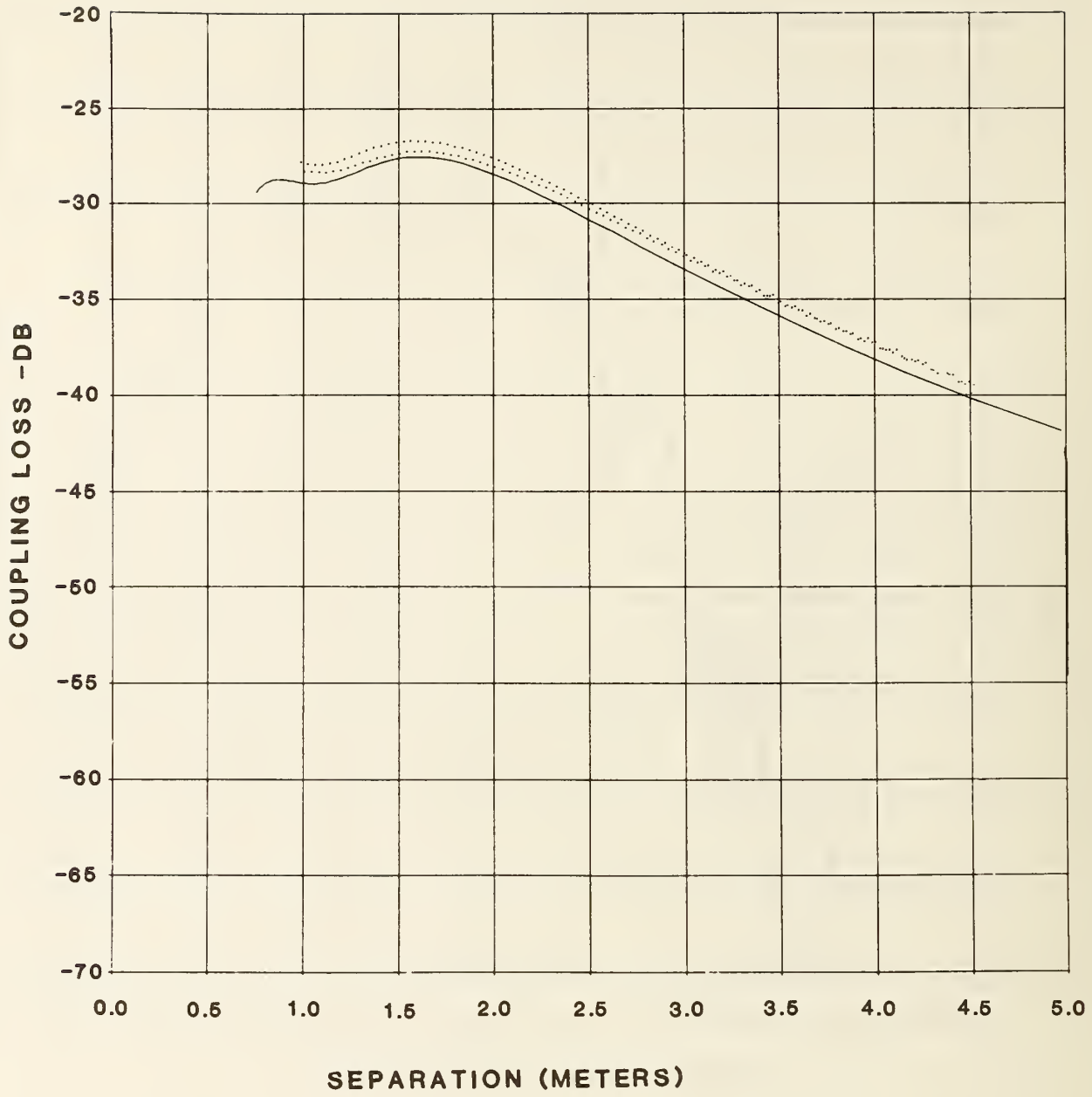

Figure 20. Comparison of measured and calculated coupling loss vs. separation between reflector and waveguide probe antennas. θ_T = 10°, θ_R = 0°. Solid curve - calculated pattern, dotted lines indicate the envelope of the measured coupling loss.

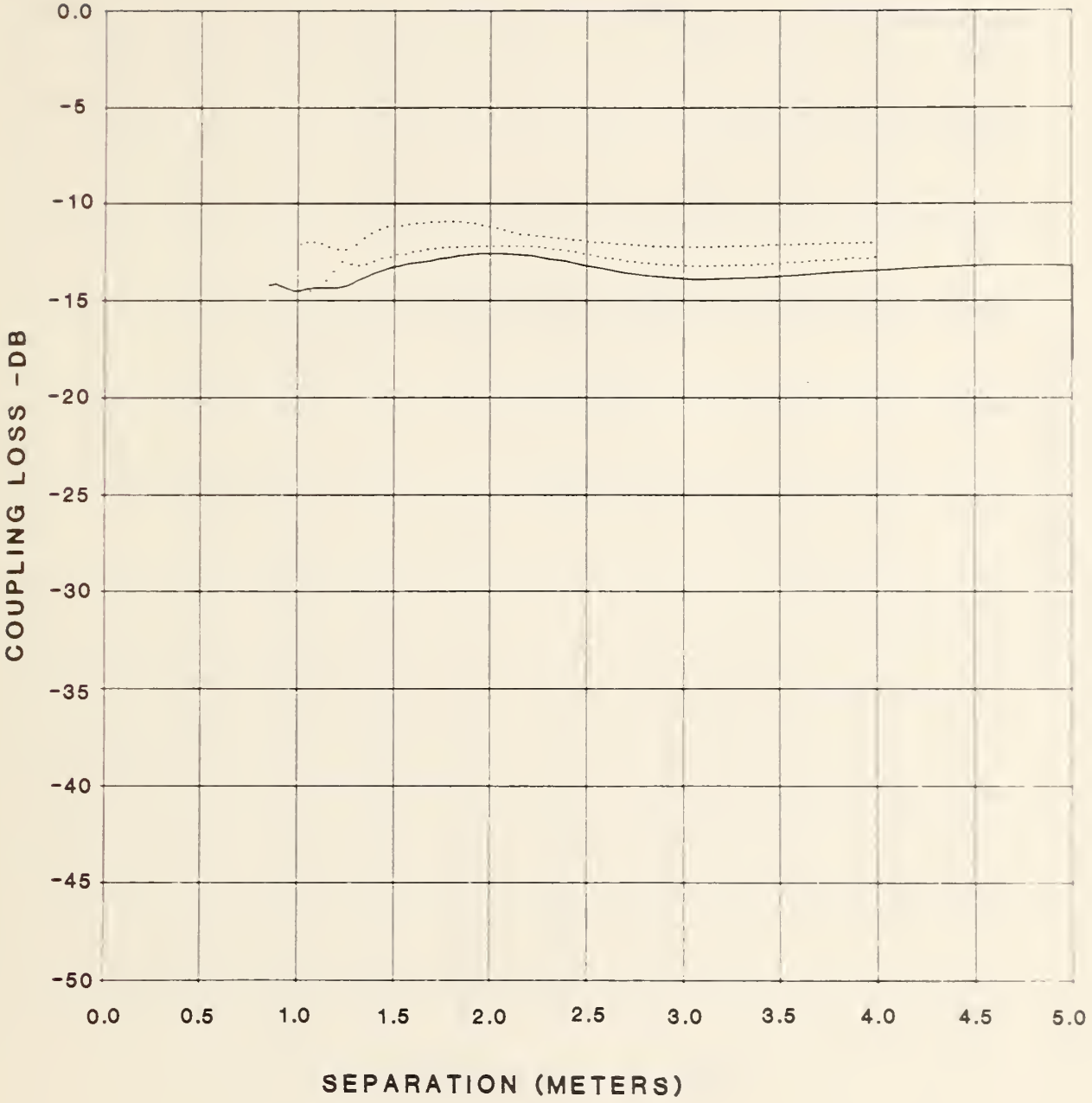

Figure 21. Comparison of measured and calculated coupling loss vs. separation between reflector and microstrip array antennas. $\theta_T = 0°$, $\theta_R = 0°$. Solid curve - calculated pattern, dotted lines indicate the envelope of the measured coupling loss.

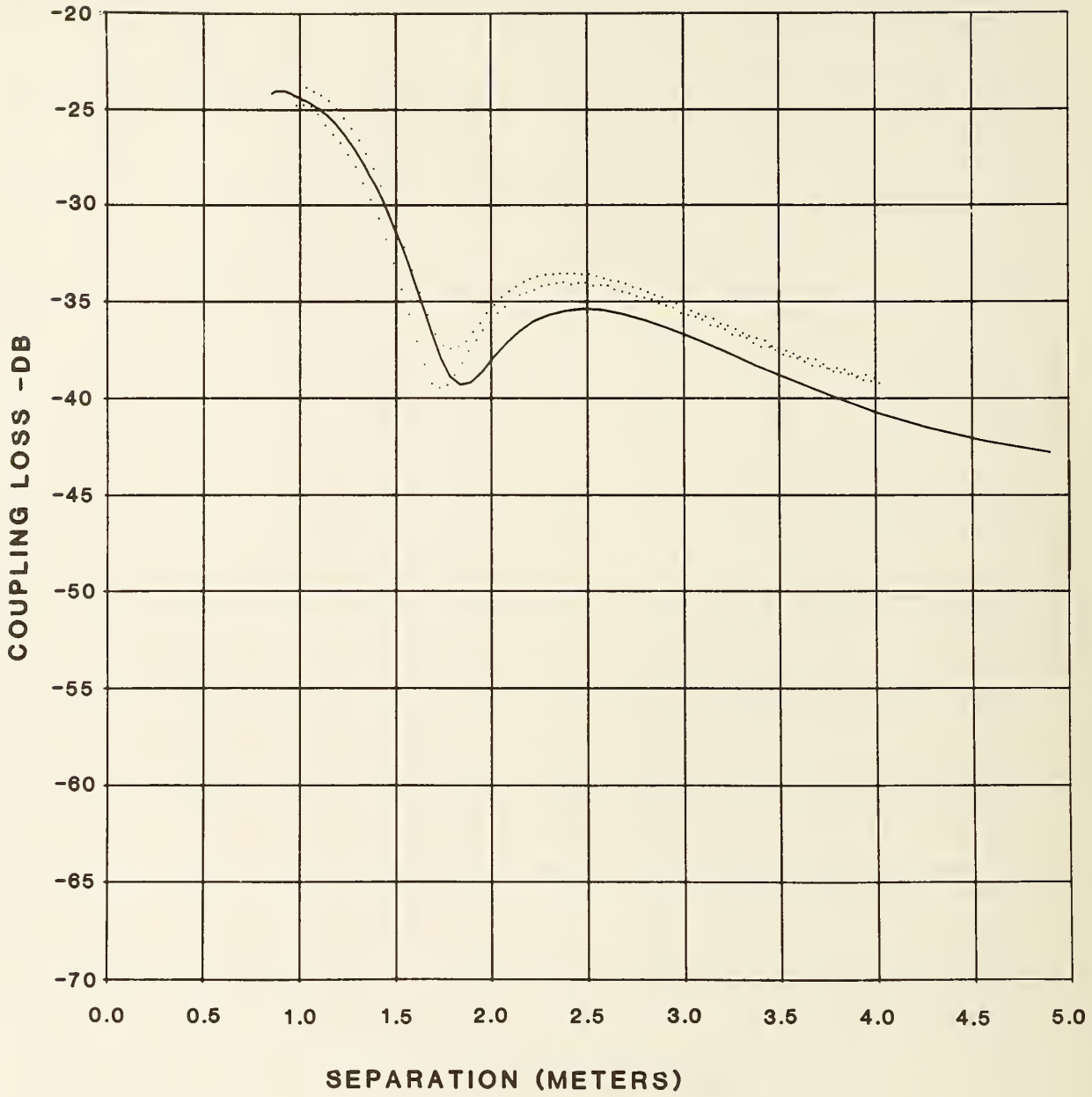

Figure 22. Comparison of measured and calculated coupling loss vs. separation between reflector and microstrip array antennas. θ_T = 20°, θ_R = 0°. Solid curve - calculated pattern, dotted lines indicate the envelope of the measured coupling loss.

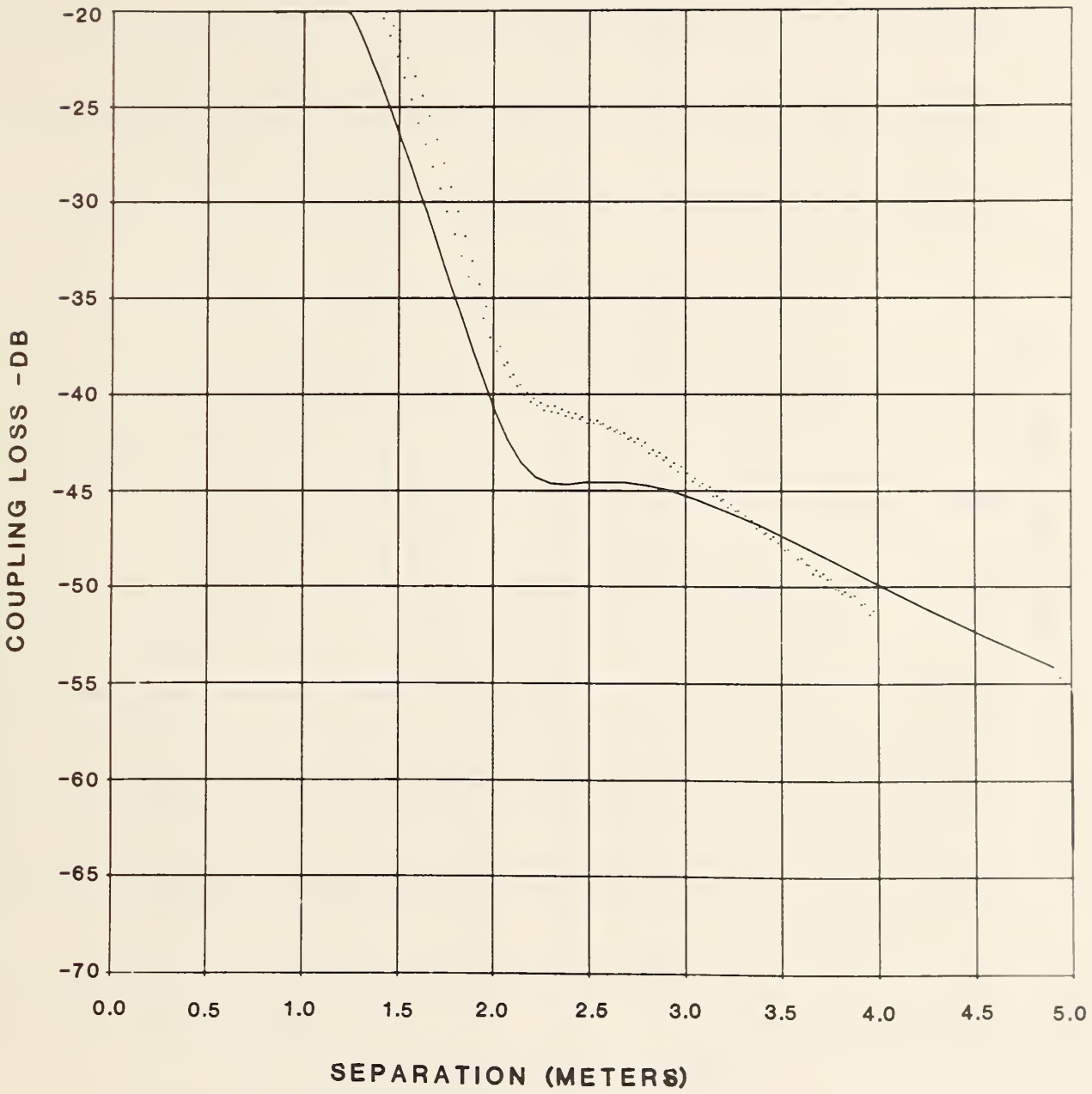

Figure 23. Comparison of measured and calculated coupling loss vs. separation between reflector and microstrip array antennas. $\theta_T = 20°$, $\theta_R = -21.6°$. Solid curve - calculated pattern, dotted lines indicate the envelope of the measured coupling loss.

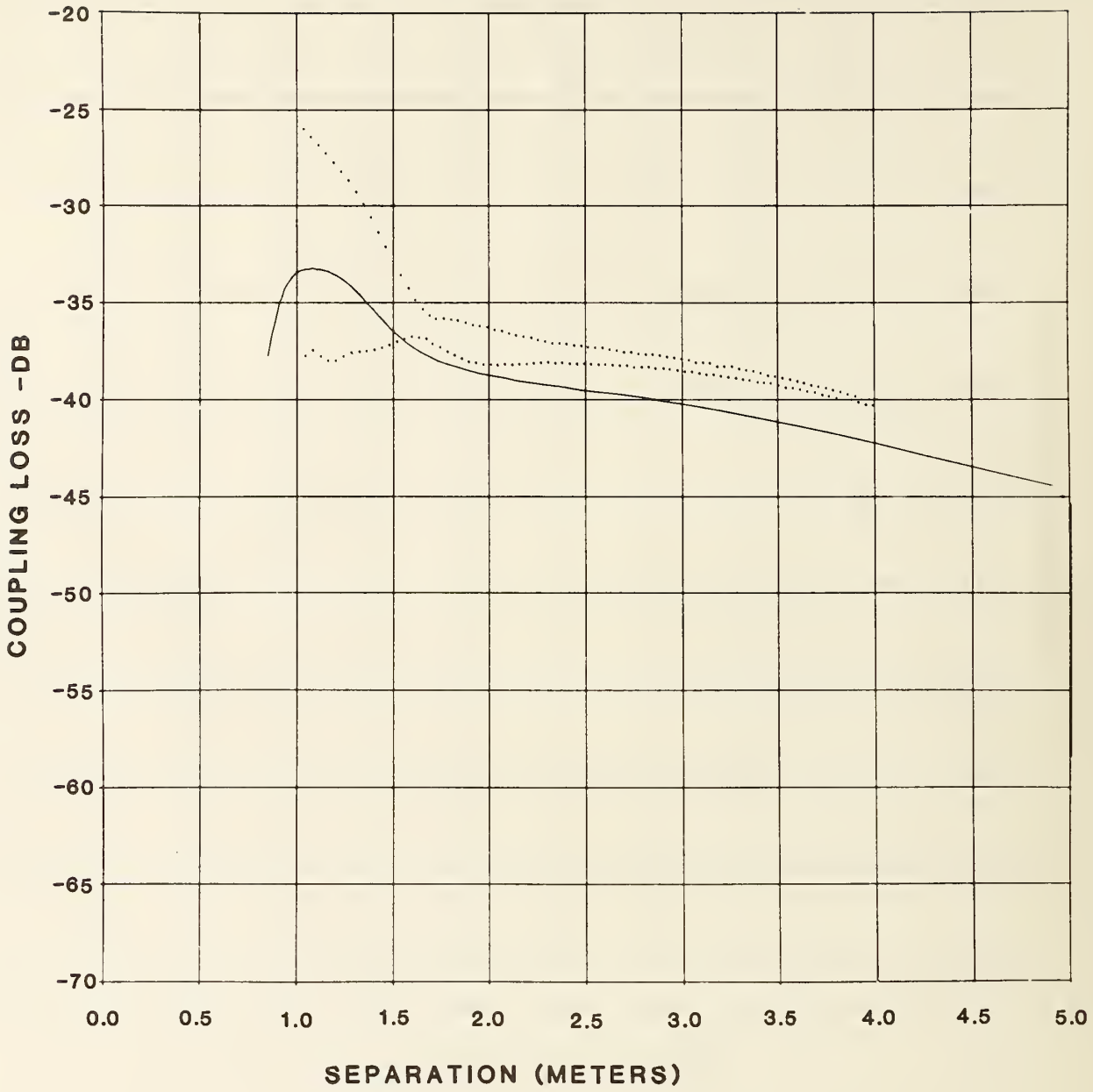

Figure 24. Comparison of measured and calculated coupling loss vs. separation between reflector and microstrip array antennas. $\theta_T = 10°$, $\theta_R = 21.6°$. Solid curve - calculated pattern, dotted lines indicate the envelope of the measured coupling loss.

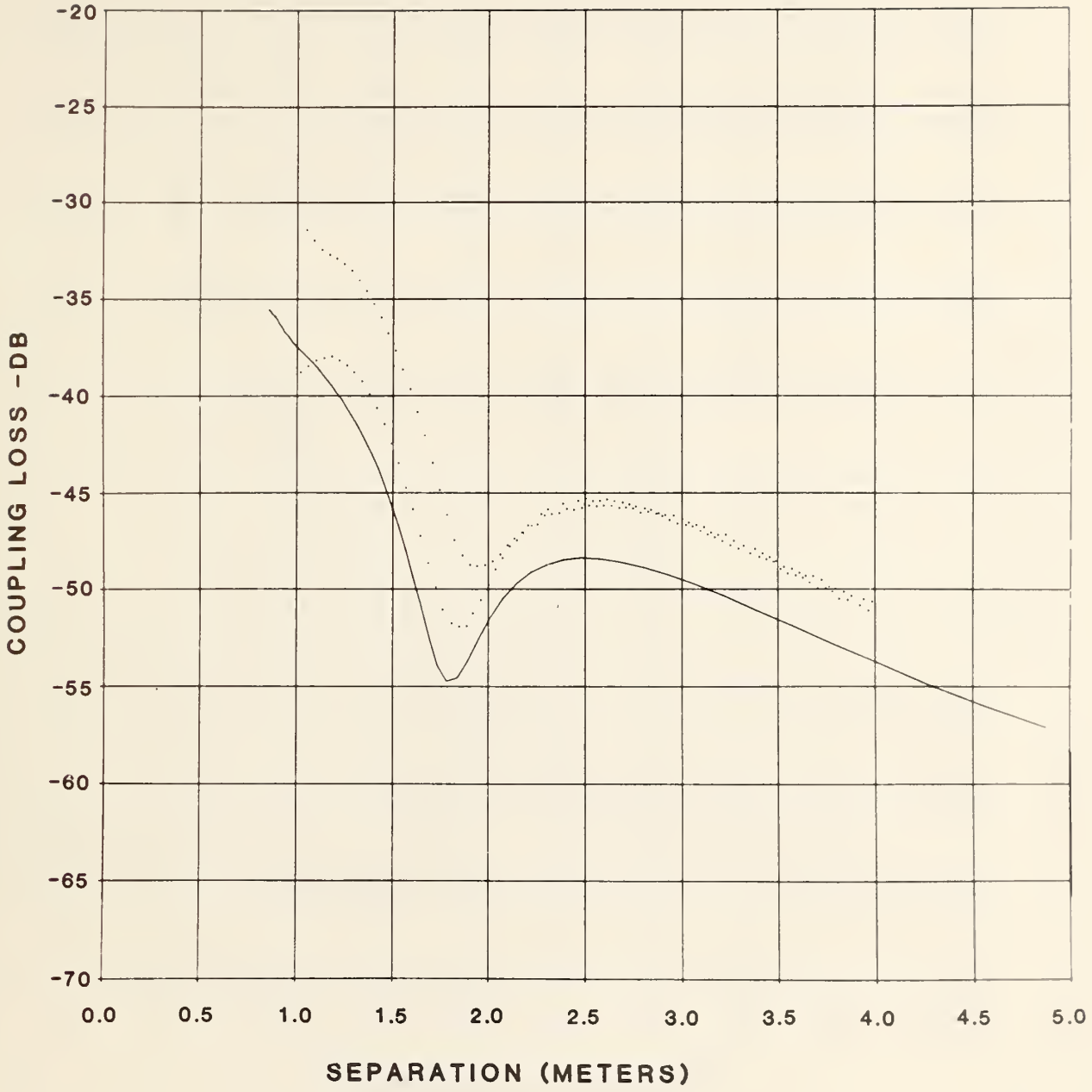

Figure 25. Comparison of measured and calculated coupling loss vs. separation between reflector and microstrip array antennas. $\theta_T = 20°$, $\theta_R = -21.6°$. Solid curve - calculated pattern, dotted lines indicate the envelope of the measured coupling loss.

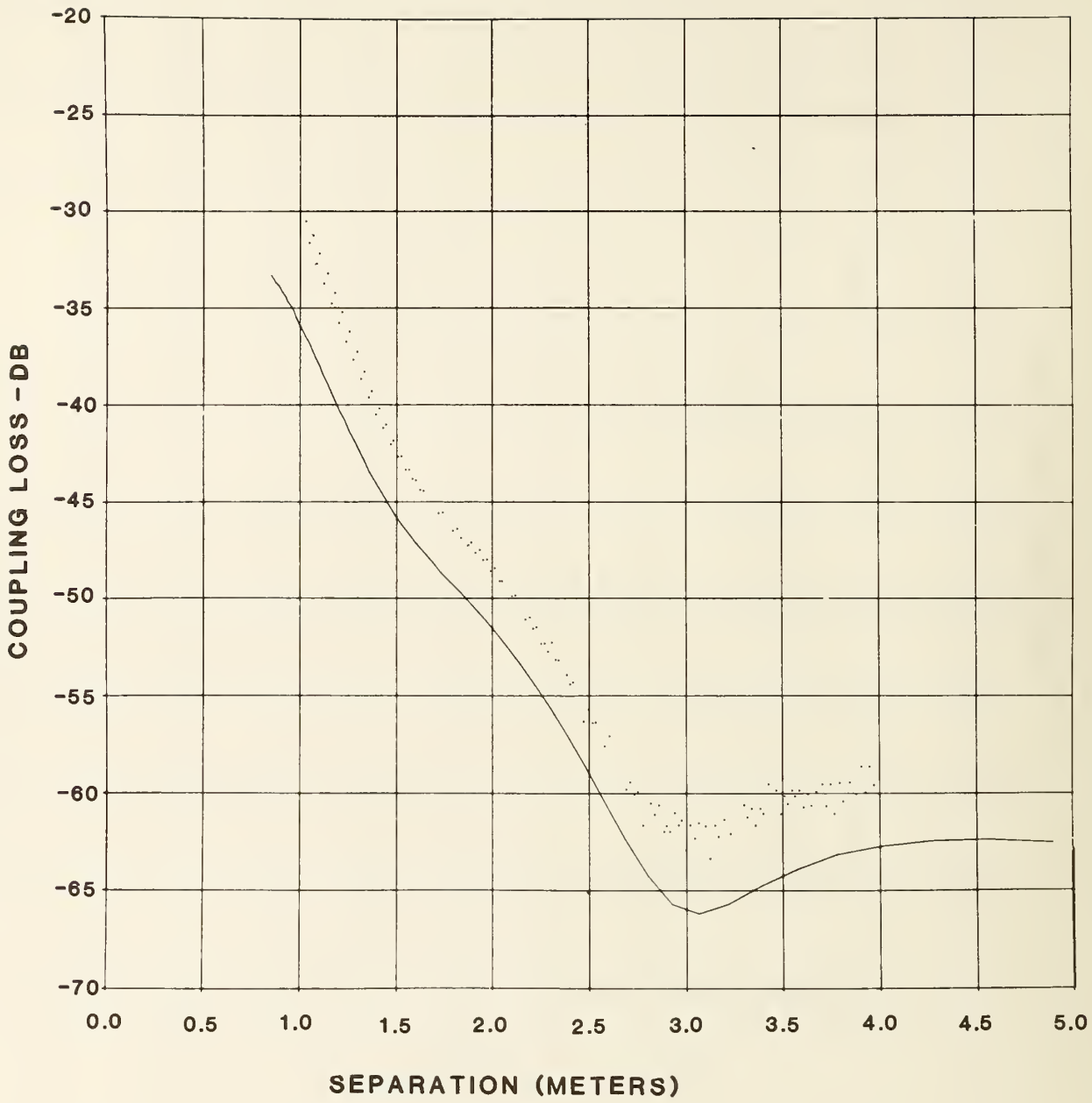

Figure 26. Comparison of measured and calculated coupling loss vs. separation between reflector and microstrip array antennas. $\theta_T = 30°$, $\theta_R = -21.6°$. Solid curve - calculated pattern, dotted lines indicate the envelope of the measured coupling loss.

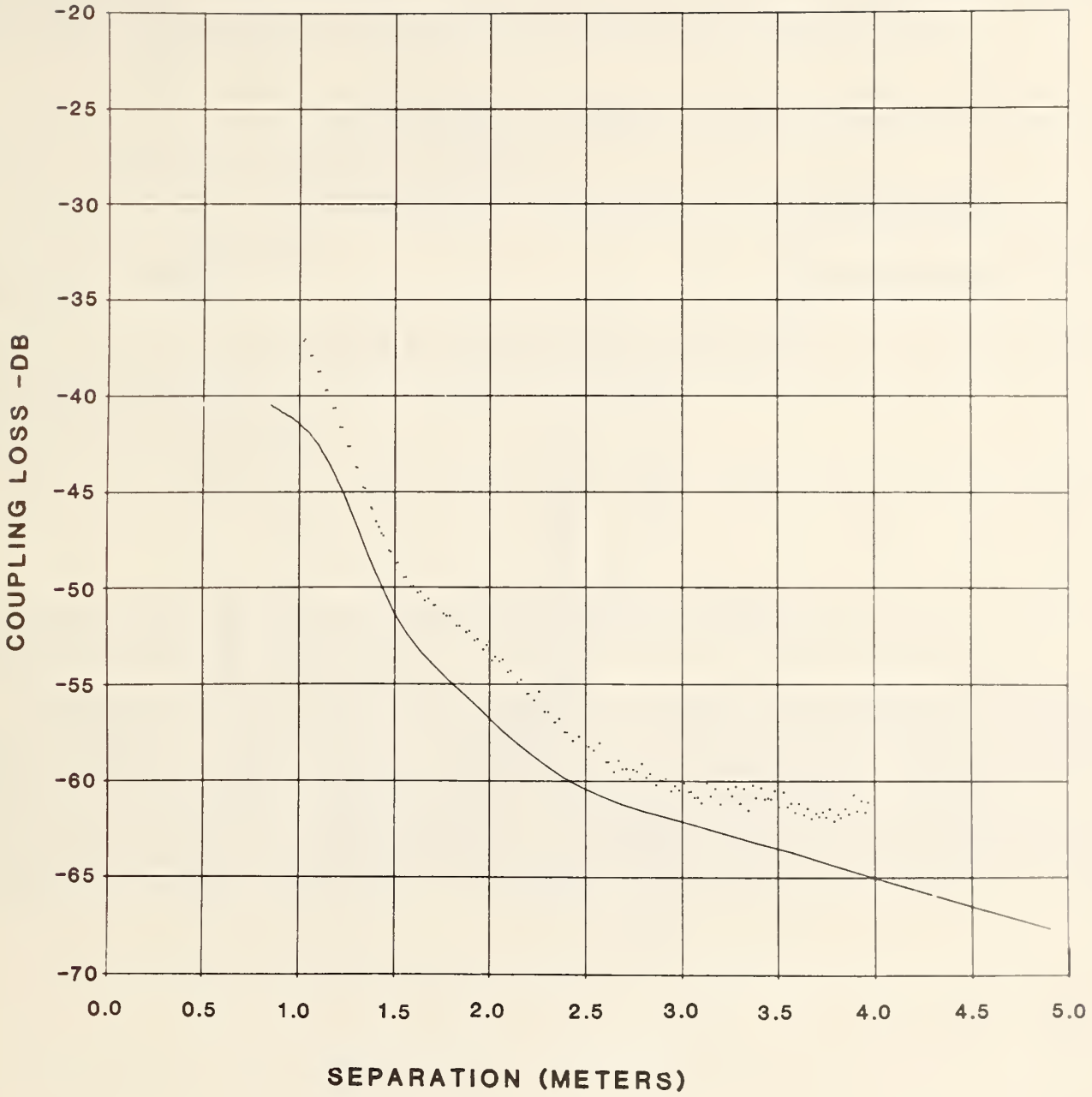

Figure 27. Comparison of measured and calculated coupling loss vs. separation between reflector and microstrip array antennas. $\theta_T = 30°$, $\theta_R = -30.3°$. Solid curve - calculated pattern, dotted lines indicate the envelope of the measured coupling loss.

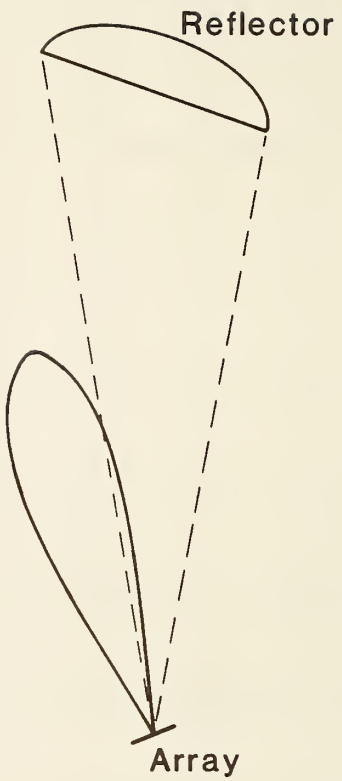

Figure 28. Drawing of the geometry for case 3 showing that a small part of the main beam of the microstrip array subtends the reflector antenna. For this reason, ENVLP correctly predicts the coupling.

NBS-114A (REV. 2-8C)

U.S. DEPT. OF COMM. BIBLIOGRAPHIC DATA SHEET (See instructions)	1. PUBLICATION OR REPORT NO. NBSIR 84-3010	2. Performing Organ. Report No.	3. Publication Date June 1984

4. TITLE AND SUBTITLE

Comparison of Measured and Calculated Mutual Coupling in the Near Field Between Microwave Antennas

5. AUTHOR(S)

Carl F. Stubenrauch and Michael H. Francis

6. PERFORMING ORGANIZATION (If joint or other than NBS, see instructions)

NATIONAL BUREAU OF STANDARDS
DEPARTMENT OF COMMERCE
WASHINGTON, D.C. 20234

7. Contract/Grant No.

8. Type of Report & Period Covered

9. SPONSORING ORGANIZATION NAME AND COMPLETE ADDRESS (Street, City, State, ZIP)

Department of Defense
Electromagnetic Compatibility Analysis Center
Annapolis, Maryland 21402

10. SUPPLEMENTARY NOTES

☐ Document describes a computer program; SF-185, FIPS Software Summary, is attached.

11. ABSTRACT (A 200-word or less factual summary of most significant information. If document includes a significant bibliography or literature survey, mention it here)

Measurements of near-field mutual coupling were performed between two moderate sized microwave antennas and compared to coupling calculated using recently developed computer programs. Input data for the programs are the complex far-field radiation patterns of the antennas. Experimentally determined and calculated coupling as a function of both transverse displacement and separation agree closely except for a constant offset observed in some cases. In addition, coupling values computed using a program which approximates the far-field radiation patterns were compared to experiment and found to be satisfactory.

12. KEY WORDS (Six to twelve entries; alphabetical order; capitalize only proper names; and separate key words by semicolons)

co-sited antennas, coupling loss, far fields, mutual coupling, near fields

13. AVAILABILITY

☒ Unlimited

☐ For Official Distribution. Do Not Release to NTIS

☐ Order From Superintendent of Documents, U.S. Government Printing Office, Washington, D.C. 20402.

☒ Order From National Technical Information Service (NTIS), Springfield, VA. 22161

14. NO. OF PRINTED PAGES 60

15. Price $10.00

U.S. GOVERNMENT PRINTING OFFICE: 1984—780-039 9390 REGION NO 8

USCOMM-DC 6043-P80